Harnessing neoantigens for targeted cancer treatment

Bulk, J. van den

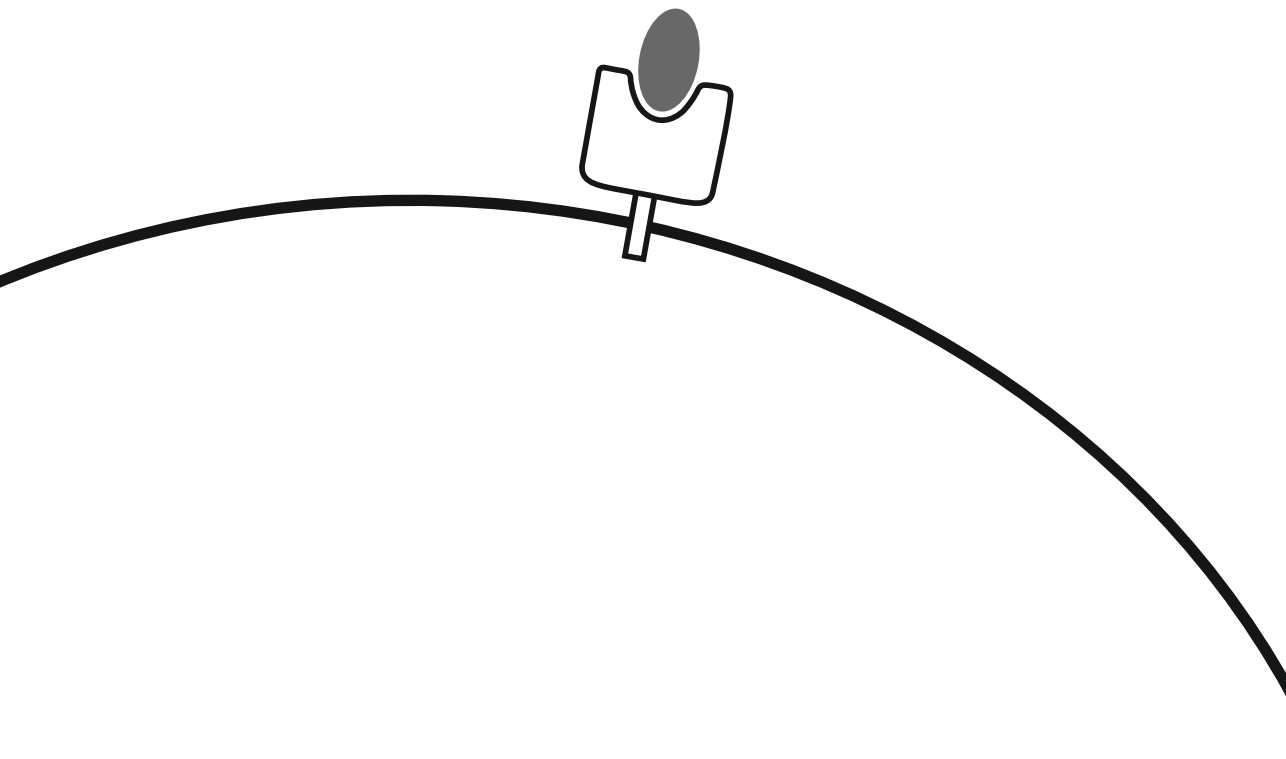

CHAPTER 3

Neoantigen-specific immunity in low mutation burden colorectal cancers of the consensus molecular subtype 4

Jitske van den Bulk, Els M.E. Verdegaal, Dina Ruano, Marieke E. IJsselsteijn, Marten Visser, Ruud van der Breggen, Thomas Duhen, Manon van der Ploeg, Natasja L. de Vries, Jan Oosting, Koen C.M.J. Peeters, Andrew D. Weinberg, Arantza Farina-Sarasqueta, Sjoerd H. van der Burg and Noel F.C.C. de Miranda

Genome Medicine. 2019;11(1):87
DOI: 10.1186/s13073-019-0697-8

ABSTRACT

Background: The efficacy of checkpoint blockade immunotherapies in colorectal cancer is currently restricted to a minority of patients diagnosed with mismatch repair deficient tumors having high mutation burden. However, this observation does not exclude the existence of neoantigen-specific T cells in colorectal cancers with low mutation burden and the exploitation of their anti-cancer potential for immunotherapy. Therefore, we investigated whether autologous neoantigen-specific T cell responses could also be observed in patients diagnosed with mismatch repair-proficient colorectal cancers.

Methods: Whole exome and transcriptome sequencing were performed on cancer and normal tissues from seven colorectal cancer patients diagnosed with mismatch repair-proficient tumors to detect putative neoantigens. Corresponding neo-epitopes were synthesized and tested for recognition by in vitro expanded T cells that were isolated from tumor tissues (tumor-infiltrating lymphocytes) and from peripheral mononuclear blood cells stimulated with tumor material.

Results: Neoantigen-specific T cell reactivity was detected to several neo-epitopes in the tumor-infiltrating lymphocytes of three patients while their respective cancers expressed 15, 21 and 30 non-synonymous variants. Cell sorting of tumor-infiltrating lymphocytes based on the co-expression of CD39 and CD103 pinpointed the presence of neoantigen-specific T cells in the $CD39^{+}CD103^{+}$ T cell subset. Strikingly, the tumors containing neoantigen-reactive TIL were classified as consensus molecular subtype 4 (CMS4), which is associated with TGF-β pathway activation and worse clinical outcome.

Conclusions: We have detected neoantigen-targeted reactivity by autologous T cells in mismatch repair-proficient colorectal cancers of the CMS4 subtype. These findings warrant the development of specific immunotherapeutic strategies that selectively boost the activity of neoantigen-specific T cells and target the TGF-β pathway to reinforce T cell reactivity in this patient group.

BACKGROUND

Colorectal cancer (CRC) is the third most common cancer worldwide and was responsible for nearly 900.000 deaths in 2018[1]. To improve cure rates for patients with advanced stage CRC, innovative treatment options are urgently needed. The recent advent of T cell checkpoint blockade-targeting immunotherapy has revolutionized the treatment of several cancers but this therapeutic modality has only been effective in CRC patients diagnosed with mismatch repair deficient (MMR-d) tumors[2-4]. MMR-d cancer cells fail to repair nucleotide substitutions as well as small nucleotide insertions and deletions that occur during DNA replication. Thereby, MMR-d tumors generally present with genomes carrying over 10 mutations per megabase, resulting in the expression of hundreds of proteins carrying non-synonymous mutations. Their immunogenic character and sensitivity to checkpoint blockade is considered to be largely derived from the recognition of somatically mutated antigens (neoantigens) by autologous T cells[5-8], in line with the strong association between mutation burden and clinical responses to checkpoint blockade in different types of solid cancers[3,4,8-11]. However, the majority of CRC (up to 80% of cases) comprise mismatch repair proficient (MMR-p) tumors with low to moderate mutation burden and are currently not amenable to immunotherapeutic interventions. CRC can also be classified according to their transcriptional profiles into consensus molecular subtypes (CMS) that carry biological and clinical significance[12]. CMS1 is dominated by MMR-d CRC with strong immune infiltration, while CMS2 and CMS3 are characterized by Wnt pathway activation and metabolic dysregulation, respectively. Lastly, CMS4 is defined by a mesenchymal signature where the stromal compartment and TGF-β signaling play a major role. Of note, patients diagnosed with CMS4 CRC have worse survival than patients diagnosed with the other subtypes[13].

The activation of an effective anti-tumor immune response requires cancer antigens to be taken up and processed by antigen presenting cells (APCs) which in turn present antigen-derived peptides to $CD8^+$ and $CD4^+$ T cells in complex with HLA class I and II molecules, respectively[14]. The molecular features of neoantigens and their affinity to the various intermediates of the antigen processing pathway determines whether they will be presented at the cell surface[15]. Therefore, the probability that a neoantigen is presented to a cognate T cell is reduced in cancers with low mutation burden, such as MMR-p CRC, thereby explaining why the clinical applicability of reactivating anti-cancer T cell responses has been mainly restricted to MMR-d CRC.

Nevertheless, the priming of neo-epitope-specific T cells in these cancers, despite their low mutation burden, would support the development of neoantigen-specific immunotherapeutic strategies, including neoantigen vaccination or adoptive transfer of neoantigen-specific T cells[16-18]. To address this possibility, we investigated the presence of neoantigen-specific T cell responses in tumor-infiltrating lymphocytes (TIL) and peripheral blood lymphocytes (PBL) of seven MMR-p CRC patients. In parallel, we characterized

the immunophenotypes of these tumors by multispectral immunofluorescence imaging. Neoantigen-specific T cell reactivity could be detected in three out of seven MMR-p cases, all with a CMS4 transcriptional profile, which is associated with worse clinical prognosis[12]. This finding supports the design of specific immunotherapeutic strategies that target neoantigens in this patient group and suggests that an increased number of CRC patients could benefit from immunotherapeutic interventions.

METHODS

Collection of patient material

This study was approved by the Medical Ethical Committee of the Leiden University Medical Centre (protocol P15.282) and all patients provided informed consent. Methodological procedures as well as clinical stage, tumor location and MMR status of the nine patients that underwent whole-exome and transcriptome sequencing are summarized in Figure 1A, 1B. MMR status was determined initially through diagnostic procedures by making use of PMS2 and MSH6 immunodetection and was further confirmed by the observation of numerous nucleotide insertions and deletions by exome sequencing in the samples classified as MMR-d. Patient samples were anonymized and handled according to the medical ethical guidelines described in the Code of Conduct for Proper Secondary Use of Human Tissue of the Dutch Federation of Biomedical Scientific Societies. This research was conducted according to the recommendations outlined in the Helsinki declaration.

Blood samples were obtained prior to surgery. Peripheral blood mononuclear cells (PBMC) were isolated from patients' heparinized venous blood by Ficoll-Amidotrizoate (provided by the LUMC pharmacy) gradient centrifugation. Tumor material and respective normal colorectal samples were obtained immediately after surgery under supervision of a pathologist. A fraction of the tumor samples was snap-frozen, another part was cut into small fragments and digested using 1 mg/mL collagenase D (Roche, Basel, Switzerland) and 50 mg/mL DNAse I (Roche) in IMDM medium (Lonza BioWhittaker, Breda, The Netherlands) supplemented with 2 mM Glutamax (Thermo Fisher Scientific, Waltham, MA, US), 20% Fetal Bovine Serum (Sigma-Aldrich, Saint Louis, MO, US), 1% penicillin/streptomycin (Thermo Fisher Scientific), 1% Fungizone (Thermo Fisher Scientific), 0.1% Ciprofloxacin (provided by the LUMC pharmacy), and 0.1% Gentamicin (Sigma-Aldrich). Tissue fragments were incubated for 30 minutes at 37°C interrupted by three mechanical dissociations on a gentleMACS Dissociator (Miltenyi Biotec, Bergisch Gladback, Germany) in gentleMACS C tubes (Miltenyi Biotec), and subsequently processed through a 70 mm strainer (Miltenyi Biotec). Single cell digests and remaining tumor fragments were cryopreserved for analysis and culturing at later stages. Additionally, 6-12 tumor fragments were directly employed for culturing of tumor-infiltrating lymphocytes (TIL).

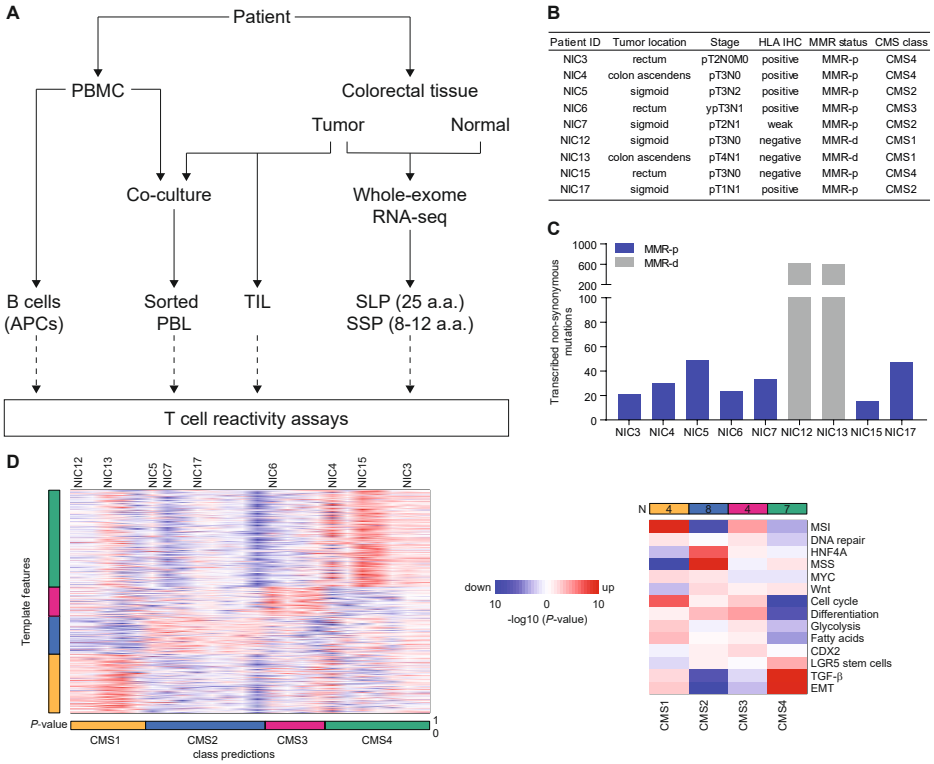

Figure 1 | *Neoantigen detection in low mutation burden CRC. (A) Schematic overview of the experimental design. (B) Patient characteristics including HLA class I phenotypes and MMR status of the tumors. (C) Total number of transcribed, non-synonymous mutations per patient. (D) Heatmaps showing the relative expression for template genes (left) and gene set (right) used to determine the Consensus Molecular Subtypes of CRC samples. Color saturation indicates the statistical significance; red and blue indicate the direction of change. The samples analyzed included the tumors that were investigated for neoantigen reactivity and additional 15 CRC samples for which RNA sequencing was available in-house.*

Whole-exome and RNA sequencing of tumor and corresponding normal tissue

Sequencing libraries were prepared from genomic DNA isolated from snap-frozen samples of tumor and corresponding normal colorectal tissue. NEBNext Ultra II DBA Library Prep kit for Illumina (New England Biolabs, Ipswich, MA, US) and IDT xGEN Exome target kit (Integrated DNA Technologies, Leuven, Belgium) were used according to the manufacturer's instructions for preparation of exome libraries. NEBNext Ultra Directional RNA Library Prep kit for Illumina (New England Biolabs) was used according to the manufacturer's instructions to generate RNA sequencing libraries. rRNA was depleted from total RNA using the NEBNext rRNA depletion kit (New England Biolabs). The obtained paired-end, 150 basepair libraries were sequenced at GenomeScan (Leiden, The Netherlands) on a

HiSeq4000 Illumina, aimed at generating 11Gb and 15Gb datasets per sample for exome and transcriptome libraries, respectively.

For exome sequencing, reads were mapped against the human reference genome (hg38) using the Burrows-Wheeler Aligner 3 algorithm (BWA-mem version 0.7.15)[19]. Duplicate reads were removed using Picard Tools[20]. Genome Analysis Toolkit 7 (GATK version 3.8; Broad Institute, Cambridge, MA, US) was used for base quality recalibration. Optitype was used to genotype HLA class I alleles from RNA and exome sequencing data (Additional file 1: Table S1) (21). Subsequently, variant calling was done using a combination of three software tools, muTect 2, varScan 2 and Strelka[22-24]. The resulting .vcf files were then combined into a single file using GATK CombineVariants[25]. Integrative Genomics Viewer (IGV, Broad Institute) was used for visual inspection of the variants[26-28]. Variants were functionally annotated using the Ensembl Variant Effect Predictor (VEP)[29]. With exception of synonymous substitutions, all other coding variants were further investigated if at least one read displaying a mutation was present in the RNA sequencing data. To this purpose, RNA sequencing reads were first mapped against the same hg38 genome build using gsnap[30], followed by read count at variant positions using the samtools mpileup tool. Allele frequencies at DNA level were extracted from the .vcf files and an mpileup file was generated for all mutated sites to inform on the number of variant-supporting reads at RNA level. Purity estimates of the tumor content were determined using Sequenza[31].

25-mer peptide sequences were generated for all the identified variants. In case of frameshifts and stop loss mutations several peptides were generated which overlapped for at least half of the sequence. Furthermore, affinity prediction of short peptides (8-12mers) to the patients' HLA alleles was performed using NetMHC 4.0 and NetMHCpan 4.0, defining top-ranked strong and weak binders[32-34]. All long peptides corresponding to mutations as well as short peptides classified as strong binders (0.5% top rank) were synthesized by the Cell and Chemical Biology department at the Leiden University Medical Center. In addition, for those variants without any strong binders, the short peptide with highest binding affinity to any HLA class I allele was also tested (Additional file 2: Table S2).

CMS classification and immune signatures

CMScaller R package was used for both Consensus Molecular Subtyping (CMS) and Gene Set Analysis (GSA) on the colorectal cancer TCGA dataset and our own cohort (Leiden cohort)[35]. For the TCGA dataset, HTSeq counts from 449 primary tumors (one per sample) were downloaded from the Genomic Data Commons portal (https://portal.gdc.cancer.gov/). For the Leiden cohort, gene expression counts were obtained using HTseq-count[36]. GSA was performed on both datasets for the 14 transcriptional signatures described by Eide and colleagues[35] and an immune-regulatory gene set that was designed based on the Molecular Signatures Database IMMUNE_RESPONSE gene set (http://software.broadinstitute.org/gsea/msigdb/cards/IMMUNE_RESPONSE, Additional file 3: Table S3). Differential gene expression between the CMS2/3 groups and the CMS4

samples was investigated on the TCGA cohort by employing the Limma-Voom package after TMM normalization of the HTseq counts with the edgeR package[37,38]. Genes were considered differentially expressed if they had a log2 fold-change below or above -1 and 1, respectively, and an adjusted P-value lower than 0.05. The immune-regulatory genes that were shown to be differentially expressed in the TCGA dataset were further investigated in the Leiden cohort.

T cell expansion and B cell immortalization

TIL expansion was performed by culturing tumor fragments in a 24-well plate with T cell medium (IMDM (Lonza BioWhittaker), supplemented with 7.5% heat-inactivated pooled human serum (Sanquin, Amsterdam, The Netherlands), penicillin (100 IU/mL), streptomycin (100 µg/mL) and L-glutamine (4 mM) both from Lonza Biowhittaker) and rIL-2 (1000 IU/mL; Aldesleukin, Novartis). After 14-21 days of culturing, TIL were harvested and cryopreserved for later use. Rapid expansion of TIL was performed to increase the number of T cells available for reactivity assays. The expansion was induced by culturing the TIL with rIL-2 (3000 IU/mL), OKT3 (Miltenyi Biotec, 30 ng/mL), and irradiated (40 Gy) feeder cells (100-200 fold excess) for 4-5 days. Feeder cells were PBMC, derived from healthy donor blood provided by Sanquin (The Netherlands), and isolated by density centrifugation with Ficoll, as described for the patients' blood. Subsequently, culturing was continued up to two weeks in T cell medium with rIL-2 (3000 IU/mL)[18]. Phenotyping of the expanded TIL was performed by flow cytometric analysis of CD4, CD8, FoxP3, CD45RA, CD45RO, CD39, CD103, and PD-1 expression (Additional file 4: Table S4A). Cells were incubated for 45 minutes with the cell surface antibodies and a live/dead marker. Subsequently, cells were treated with the Transcription Factor Staining Buffer Set (eBioscience, San Diego, CA, US) to prepare cells for FoxP3 detection. Samples were measured on an LSRFortessa machine (BD, Franklin Lakes, NJ, US) and the data was analysed using FlowJo software v10.2 (BD).

Epstein-Barr virus–transformed lymphoblastoid B cell lines (EBV-LCL) were used as antigen-presenting cells (APCs). Their immortalization was induced by incubating patients' PBMC with supernatant of the marmoset B cell line containing infectious particles of EBV strain B95-8 for 1h at 37°C. Culture medium consisted of RPMI-1640, supplemented with 5 µg/mL PHA (Thermo Fisher Scientific), 10% FCS, L-glutamine (4 mM), penicillin (100 µg/mL) and streptomycin (100 µg/mL). Cells were refreshed every 5-6 days with B cell medium and cultured for three weeks before being used as APCs.

Tumor-reactive lymphocytes from peripheral blood were generated by co-culture of PBMC with lethally irradiated (100 Gy) tumor fragments in T cell medium and subsequent isolation of PD1-positive cells[39]. Cells were harvested and stained with PE-labelled anti-PD1 antibodies (BD Biosciences). Next, MACS cell sorting was performed by use of magnetic anti-PE beads (Miltenyi Biotec) and MS columns (Miltenyi Biotec). PD-1-positive cells as well as flow-through were expanded as described above for the TIL cultures. Cul-

ture medium containing rIL-2 was refreshed on alternate days. Cells were cryopreserved after a culturing period of two weeks.

$CD39^{+}CD103^{+}$ $CD8^{+}$ T cell fractions were sorted and cultured as described previously[40]. In short, single cell suspensions derived from tumor digests were stained to perform a flow cytometric cell sort of the cell types of interest based on phenotypic markers using the following antibodies: CD45 FITC (BioLegend, San Diego, CA, US; 2D1); CD4 BV785 (BioLegend); CD8 BV510 (BioLegend, RPA-T8); CD45RA APC-780 (eBioscience, San Diego, CA, US; HI100); CCR7 PE/Dazzle 594 (BioLegend, G0443H7); CD39 APC (eBioscience, eBioA1); CD103 PE (eBioscience, B-Ly). The sorted cells were cultured in RPMI-1640, supplemented with 2mM glutamine, 1% non-essential amino acids, 1% sodium pyruvate, penicillin (50 IU/mL), streptomycin (50 µg/mL) and 10% fetal bovine serum (Hyclone, South Logan, UT, US). T cells were stimulated with 1 µg/mL PHA (Remel) in the presence of irradiated (40 Gy) allogeneic feeder cells ($2*10^5$ cells/well) and 10 ng/mL IL-15 (BioLegend) in a 96-well round-bottom plate. The T cells were maintained in complete medium containing IL-15 until cryopreservation.

T cell reactivity

Reactivity of T cells to tumor material and/or neoantigens was investigated by a co-culture reactivity assay. In order to screen for neoantigen reactivity, autologous EBV-LCL were placed in overnight co-culture with 20 µg/mL of synthetic long peptides (SLP). Synthetic short peptides (SSP) were directly added at a concentration of 2 µg/mL to T cells, without addition of EBV-LCL. Fifteen-thousand T cells were tested per condition including overnight co-cultures with irradiated (60 Gy) tumor material, SSP, or 30.000 EBV-LCL loaded with SLP. Unloaded EBV-LCL or medium supplemented with and without DMSO corresponding to the peptide solution, served as negative controls. *Staphylococcus aureus* enterotoxin B (SEB; 0.5 µg/mL; Sigma-Aldrich) was used as positive control. T cell reactivity was primarily determined by IFN-γ secretion in the supernatant, measured by ELISA (Sanquin or Mabtech, Stockholm, Sweden). In addition, CD137 expression on T cells, measured by flow cytometric analysis with a panel targeting CD3, CD4, CD8, CD137 and a live/dead marker, was used as an activation read-out. Antibody details and the settings of the LSRFortessa machine (BD, Franklin Lakes, NJ, US) can be found in Additional file 4: Table S4B. To detect reactivity against tumor material, granzyme B secretion was also assessed by ELISA (Mabtech) and T cells were harvested for RNA isolation with Nucleospin RNA XS kit (Macherey Nagel, Düren, Germany), according to manufacturer's instructions. Gene expression was measured by qPCR with the SsoFast Evagreen Supermix (Bio-Rad, Hercules, CA, US) and the following primer pairs: IFNG Fw ACACTCTTTTGGATGCTCTGGT; IFNG Rv TTGGAAAGAGGAGAGTGACAGAA; GZMB Fw GATGCAGGGGAGATCATCGG; GZMB Rv CCGCACCTCTTCAGAGACTT; TNFRSF9 AGAGAGGTCGGCTGGAGATG; TNSRSF9 Rv CCCTGGACAAACTGTTCTTTGGA.

Immunohistochemistry and immunofluorescence

Formalin-fixed, paraffin-embedded tissue slices of 4 µm were cut on glass slides for immunohistochemical or immunofluorescence detection. Tissue sections were deparaffinized by xylene and rehydrated by decreasing concentrations of alcohol solutions. Endogenous peroxidase was blocked with 0.3% hydrogen peroxide in methanol solution for 20 minutes. Pre-treatment of the sections included heat-induced antigen retrieval in pH 6.0 citrate buffer (10 mM, not used for β2-microglobulin detection). Primary antibodies were diluted in PBS with 1% BSA and incubated overnight. Three antibodies against the heavy and light chains of the HLA class I molecules (HCA2 1:3200 (Nordic MUbio, Susteren, The Netherlands), HC10 1:3200 (Nordic MUbio) and β2-microglobulin (B2M) 1:100 (Dako, Carpinteria, CA, US) were used for immunohistochemical detection. The secondary antibody, a polymeric HRP-linker antibody conjugate (Immunologic, Duiven, The Netherlands) was incubated for 1h, followed by development using DAB+chromogen (Dako) for 5 minutes. Counterstaining was performed with hematoxylin for 30 seconds. Finally, sections were dehydrated by increasing amounts of alcohol followed by xylene. Slides were mounted using Pertex. Expression of HLA class I was assessed in every tumor section using the scoring system: positive, negative or weak[41]. Scoring took place against the internal control, provided by stromal and immune cells.

For T cell infiltrate analysis, additional tissue sections were used for immunofluorescence detection of Keratin, CD3, CD8, and FoxP3 as previously reported[42]. In short, pH 6.0 citrate buffer was used for heat-induced antigen retrieval. Superblock buffer (Thermo Fisher Scientific) was applied and, subsequently, all primary antibodies that were detected indirectly by isotype-specific fluorescent-labelled antibodies were incubated overnight (CD8 and FoxP3). Then, the secondary antibodies were applied, followed by incubation with the directly conjugated antibodies (CD3-AF594 and Keratin-AF488). Finally, a nuclear counterstain was performed with 1 µM DAPI. Analysis was performed using the Vectra 3.0 Automated Quantitative Pathology Imaging System (Perkin Elmer, Waltham, MA, US) which captured 20x magnification images. The software was trained to segment tissues into tumor, stroma and 'no tissue' areas, followed by cellular segmentation. Subsequently, the software assigned phenotypes to all cells according to the expression of the markers employed. Cell counts were normalized by tissue area (number of cells/mm^2).

Statistics

Student's *t* test was applied to test differential reactivity to wild-type and mutant peptides with Bonferroni's correction for multiple testing. One-way ANOVA was employed for detecting differences in granzyme B secretion upon co-culture of TIL with tumor fragments. These tests and graphical representation were performed with Graphpad Prism 8.0.1.

RESULTS

The neoantigen landscape of mismatch repair proficient colorectal cancers

We determined the mutational profiles of seven mismatch repair-proficient (MMR-p) and two mismatch repair-deficient (MMR-d) CRC by whole-exome and transcriptome sequencing of cancer tissues and respective normal colonic mucosa (Figure 1A, 1B). All non-synonymous (i.e. missense mutations, nucleotide insertions and deletions leading to frameshift and non-frameshift mutations, stop loss mutations, and splicing mutations) somatic mutations were considered as potential neoantigens. We identified 15 to 49 transcribed, non-synonymous somatic mutations in MMR-p CRC (Figure 1C). In comparison, the same approach led to the discovery of approximately 20 times more mutations in the MMR-d cancers. Patient-specific HLA class I alleles were typed from the transcriptome and whole-exome sequencing data generated from tumor and healthy tissues which showed full concordance (Additional file 1: Table S1).

HLA class I expression in cancer tissues was investigated by immunohistochemistry with antibodies against the HLA class I heavy-chain. Membranous HLA class I expression was retained in the majority of MMR-p cancers while lost in NIC15 (MMR-p tumor) and both MMR-d samples (Figure 1B). This indicates that the antigen processing machinery is still operational in most MMR-p tumors. No genetic basis for loss of HLA class I expression in sample NIC15 could be found after analysis of the exome and RNA sequencing data while frameshift mutations in the *HLA-A* (NIC12 and NIC13) and *CANX* (NIC13) genes were discovered in the MMR-d samples. Transcriptome analysis of the NIC samples together with an additional 15 CRC samples (Leiden cohort) was used to classify the tumors according to the consensus molecular subtypes of CRC[35]. In accordance with their MMR-d status, NIC12 and NIC13 were classified into the CMS1 subtype, while the MMR-p samples were classified as belonging to the CMS2, 3 or 4 subtypes (Figure 1D).

Detection of neoantigen-specific T cell responses in low mutation burden CRC

Neoantigen recognition in the MMR-p cancers was tested by stimulation of the different T cell cultures with SSP and EBV-LCL loaded with SLP (Figure 1A). T cell reactivity was measured based on IFN-γ production as detected by ELISA, and expression of the activation marker CD137, assessed by flow cytometry.

An initial screening revealed potential neoantigen-reactivity in six out of the seven MMR-p CRC in both TIL and PBL-derived T cell cultures (Figure 2A; Additional file 5 and 6: Fig. S1 and Fig. S2). High IFN-γ production was observed when PBL-derived T cells were co-cultured with EBV-LCL in all samples, except NIC6, irrespective of the SLP loading. A similar observation was done with the TIL product of NIC5 and NIC17, suggesting the presence of EBV-reactive cells in these T cell products. Potential hits identified in the

previous screen were validated with HPLC-purified, wild type and mutant versions of the putative neoantigen sequences. A *bona fide*, neoantigen-specific T cell response was defined when T cells specifically reacted against the mutant peptide. Neoantigen-specific T cell reactivity was observed in the samples derived from patients NIC3, NIC4, and NIC15 (Figure 2B; Additional file 7: Fig. S3). For NIC3, T cell reactivity was confirmed against two SLP representing the mutations *PARVA* c. 328C>G (p.P110R, peptide L01) and *G3BP1* c. 244G>A (p.A82T, peptide L13) and an SSP (peptide S13-1) corresponding to the latter variant (Figure 2B, Table 1). In NIC4, T cell responses were directed towards SLP corresponding to three different mutations: *ACTR10* c.638G>A (p.R213H, peptide L06), *RAE1* c.1106A>G (p.X369W, peptide L20-2), and *PDP1* c.1024C>T (p.R342W, peptide L29) (Figure 2B, Table 1). In NIC15 T cell activity was detected towards a SLP representing the c.1054C>A (p.V352F) mutation in *QRICH1* (Figure 2B, Table 1). The targeted genes lack any apparent involvement in CRC oncogenesis but, importantly, they were present among the dominant tumor clones as determined by the mutated allele frequency and estimated tumor cell fractions (Table 1; Additional file 2: Table S2). Furthermore, the RNA expression levels of neoantigen-encoding genes were comparable to the ones of genes encoding the remaining non-recognized mutations (Additional file 8: Fig. S4A). In these patients, 20 (NIC3), 35 (NIC4) and 15 (NIC15) putative neoantigens had been identified by sequencing which translates to a neoantigen detection rate of 10%, 9%, and 6.7%, respectively. No neoantigen reactivity was observed in blood-derived T cells (Additional file 7: Fig. S3), although the analysis was likely hampered by EBV-directed background reactivity as a result of EBV-transformed B cells being employed as APCs. Furthermore, the specific selection of PD-1^{hi} subsets might have been more successful for pre-selection of tumor-specific T cells[43,44].

To investigate if the observed T cell responses were genuinely patient-specific, the TIL of NIC3 and NIC4 were stimulated with the putative neoantigen peptide pools from other patients (Additional file 9: Fig. S5). No cross-reactivity was detected, emphasizing the patient-specific nature of the detected T cell responses.

Table 1 | Patient's neo-epitopes to which T cell reactivity was detected.

Patient	% Tumor	#Mut	#SLP	#SSP	Genes	Mut cDNA	Mut a.a.	% Mut (WES)	Peptide	Peptide ID
NIC3	21	21	24	47	*PARVA*	c.328C>G	p.P110R	11	NLPLSPIPFELDREDTMLEENEVRT	L01
					G3BP1	c.244G>A	p.A82T	11	NCHTKIRHVDAHTTLNDGVVVQVMG	L13
					G3BP1	c.244G>A	p.A82T	11	IRHVDAHTTL	S13-1
NIC4	48	30	39	46	*ACTR10*	c.638G>A	p.R213H	15	SVPEGVLEDIKAHTCFVSDLKRGLK	L06
					RAE1	c.1106A>G	p.X369W	13	WWLETLAQPELFLSTLPHLCTNLGP	L20-2
					PDP1	c.1024C>T	p.R342W	45	PKSEAKSVVKQDWLLGLLMPFRAFG	L29
					PDP1	c.1024C>T	p.R342W	45	SEAKSVVKQDW	S29-1
					PDP1	c.1024C>T	p.R342W	45	SEAKSVVKQDWL	S29-2
NIC5	72	49	71	94	-	-	-	-	-	-
NIC6	79	23	24	32	-	-	-	-	-	-
NIC7	78	33	44	70	-	-	-	-	-	-
NIC15	43	15	15	108	*QRICH1*	c.1054C>A	p.V352F	14	VHVSGSPTALAAFKLEDDKEKMVGT	L11
NIC17	51	45	47	60	-	-	-	-	-	-

% Tumor – tumor purity, Mut – mutation, SLP – synthetic long peptides, SSP – synthetic short peptides, WES – reads in whole exome sequencing.

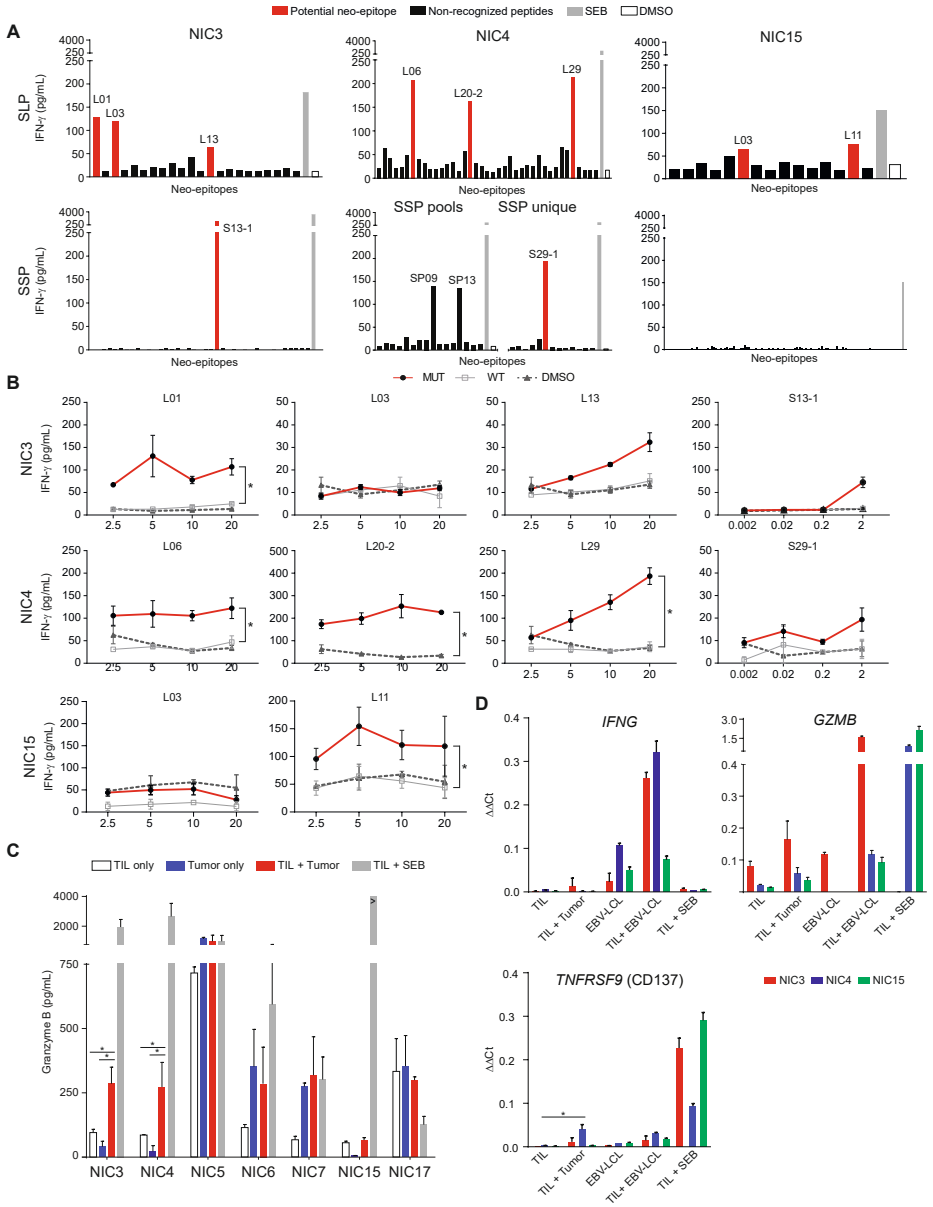

Figure 2 | *Neoantigen-specific T cell reactivity in MMR-p CRC. (A) IFN-γ production of expanded TIL in response to synthetic long peptides (SLP) and synthetic short peptides (SSP), potential neo-epitopes in red and non-recognized peptides in black. SEB (grey) and DMSO (white) were taken along as positive and negative control, respectively. Peptide IDs are included for neo-epitope responses that were judged positive and selected for validation. SSP and SLP with the same ID number correspond to the same mutation per patient. (B) IFN-γ production of TIL upon co-culture with mutant (red) and corresponding wild type (grey) peptides, and a DMSO control (dashed), at different peptide concentrations. The mean ± standard deviation of the biological duplicates in the same experiment are depicted. An asterisk indicates a significant difference (α=0.0026) between wild type and mutant*

peptides. (C) Granzyme B production by TIL upon stimulation with autologous tumor fragments (red). TIL-only (white) and tumor-only (blue) conditions were taken along as negative controls, SEB (grey) as positive control. Differential production between TIL + Tumor and TIL or Tumor only is analyzed by ANOVA, the asterisks indicate significant differences. (D) Gene expression measured by qPCR upon co-culture of different target/effector combinations of NIC3 (red), NIC4 (blue) and NIC15 (green). Differential gene expression upon co-culture with wild type and mutant peptides is indicated with an asterisk.

Tumor-directed T cell reactivity in MMR-p CRC

TIL were co-cultured with small, irradiated tumor fragments in order to assess whether tumor-directed T cell activity could be detected in the same samples where neoantigen-specific T cells were identified. Initially, tumor-reactivity was assessed in a similar manner to the neo-epitope screening and showed that the TIL cultures established from patient NIC4 produced IFN-γ upon stimulation with autologous cancer tissue. Furthermore, they also displayed increased CD137 expression in approximately 5% of $CD8^+$ T cells (Additional file 8: Fig. S4B, S4C; adjusted for negative control) indicating that tumor reactivity was restricted to a minority of TIL in this sample. Recently, other groups have reported discordance between IFN-γ production and CD137 expression in similar assays with CRC tissues, despite the true nature of neoantigen-specific reactivity[45]. To address potential issues related to the sensitivity of this approach, an additional strategy was employed to screen all samples by measuring granzyme B release in the supernatant of the co-cultures followed by gene expression analysis of TIL[46]. Granzyme B release was found to be increased compared to the negative controls in both NIC3 and NIC4 when TIL were co-cultured with tumor material (Figure 2C). The same was not observed upon co-culture of NIC15 TIL with tumor material which may be explained by the fact that this tumor had lost HLA class I expression (Figure 1B). In the same experimental setting, RNA was isolated from the different co-cultures and the expression levels of the *IFNG*, *GZMB* (granzyme B), and *TNFRSF9* (CD137) were assessed (Figure 2D). While generally supportive of tumor-directed reactivity it is striking that these genes behave differently as readouts depending on the sample but also on the type of stimuli, thus, highlighting the need to redefine comprehensive and sensitive approaches for the identification of cancer-reactive T cells in CRC.

CD39 and CD103 identify neoantigen-reactive $CD8^+$ T cells

Co-expression of CD39, an ectonucleotidase, and CD103, an integrin that pinpoints tissue-resident T cells, have been proposed to discriminate tumor-infiltrating, cancer-reactive $CD8^+$ T cells[40]. We investigated whether neoantigen reactivity in MMR-p CRC was also compartmentalized into specific $CD8^+$ T cell subsets defined by the aforementioned markers. To this end, $CD8^+$ TIL from patient NIC4 were sorted by flow cytometry into double negative, single positive, and double positive subsets according to CD39 and CD103 expression (Figure 3A). Subsequently, these populations were expanded and tested for neoantigen reactivity towards all the mutant peptides of NIC4. Neoantigen-specific responses were specifically observed in the $CD39^+CD103^+$ $CD8^+$ T cell subset. T cell

activation was detected against the L29, S29-1 and S29-2 peptides (Figure 3B), all derived from the *PDP1* c.1024C>T mutation that was shown to be recognized by T cells in the bulk TIL product (Table 1). This observation could be reproduced using HPLC-purified peptides harboring the neoantigen sequence, and its corresponding wild type sequence which did not elicit T cell activation (Figure 3C). Approximately 40% of $CD39^{+}CD103^{+}$ $CD8^{+}$ T cells expressed CD137 after being exposed to the L29 peptide, as opposed to 1.41% when using the wild type peptide (Figure 3D). For S29-1 and S29-2, CD137 expression was found in 13.9% and 2.42% of $CD39^{+}CD103^{+}$ $CD8^{+}$ T cells, respectively, compared to only 0.65% and 2.05% upon stimulation with the corresponding wild type peptide.

We did not observe reactivity against *ACTR10* c.638G>A (p.R213H) or *RAE1* c.1106A>G (p.X369W) in the sorted T cell fractions, which could possibly be explained by the fact that those responses were mediated by $CD4^{+}$ T cells. In agreement, no reactivity was detected against SSP derived from the same mutations.

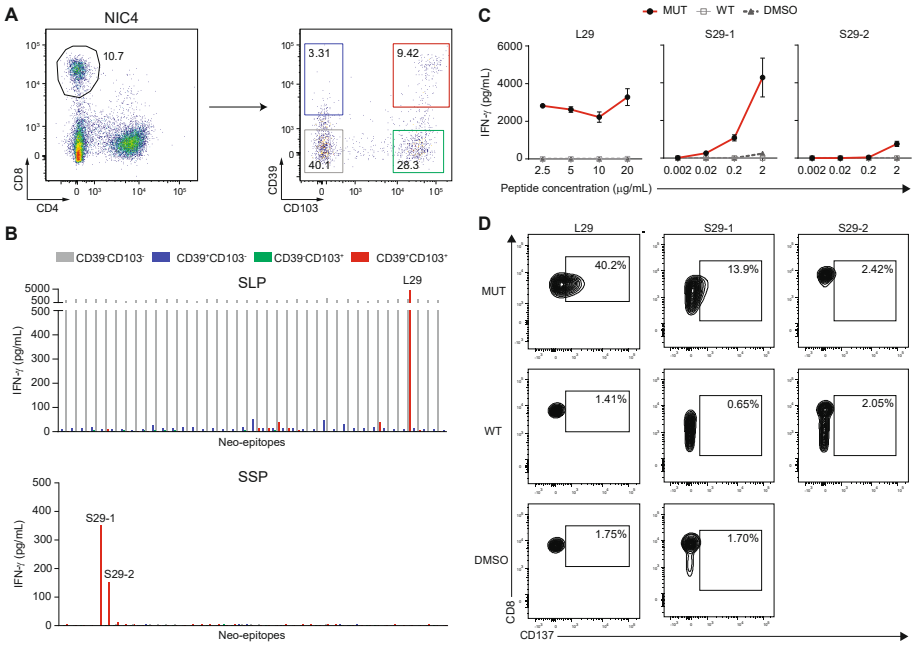

Figure 3 | *Neoantigen reactivity is contained within $CD39^{+}CD103^{+}$ $CD8^{+}$ T cell subsets. (A) Flow cytometric sorting procedure adopted for the isolation of $CD8^{+}$ T cell subsets according to CD39 and CD103 expression. Numbers within the gates represent the percentage of $CD8^{+}$ cells contained in each subset. (B) Neoantigen-specific responses of the different T cell subsets upon co-culture with neo-epitopes. Peptide numbers are included for responses that were determined to be positive, and were taken along in the validation experiment. (C) IFN-γ production of the $CD39^{+}CD103^{+}$ $CD8^{+}$ T cells upon co-culture with mutant (black) and corresponding wild type (grey) peptides, and a DMSO control (dashed), at different peptide concentrations. The mean ± standard deviation of the biological duplicates in the same experiment are depicted. (D) Flow cytometric analysis of the percentage of $CD137^{+}$ T cells, depicted in the gates, within the $CD8^{+}$ population of the expanded TIL upon co-culture with the mutant or wild type peptide, or DMSO control.*

As previously reported, T cell reactivity directed to EBV-LCL was confined to the CD39CD103$^-$ CD8$^+$ T cell subset[40,47]. In this subset, IFN-γ production was detected against all SLP-loaded and unloaded EBV-LCL (Figure 3B). This suggests that the sorting of specific T cell subsets prior to T cell expansion and T cell reactivity assays can enrich the number of tumor-specific T cells and facilitate the discovery of neoantigen-reactive T cells.

Additional single cell digests were not available for NIC3 and NIC15 and, therefore, the compartmentalization of neoantigen reactivity within specific CD8$^+$ T cell subsets could not be investigated in these samples.

T cell reactivity correlates with CMS subtype and immune cell infiltration patterns

All CRC in which neoantigen-directed T cell reactivity was detected (NIC3, NIC4 and NIC15) were classified as CMS4 according to their transcriptional profile, characterized by a strong mesenchymal signature associated with TGF-β pathway activation. The success rate of initial TIL culture and expansion, or the phenotypical constitution of TIL samples do not indicate an increased likelihood of encountering neoantigen-specific T cell responses in the CMS4 subtype (Additional file 10: Table S5). To investigate differences in the quality and quantity of T cell infiltration in the samples screened for neoantigen reactivity we performed multispectral fluorescence imaging (Figure 4A, 4B). As expected, the highest number of T cells (total and CD8$^+$ T cells) were found in the MMR-d samples NIC12 and NIC13. Interestingly, the samples with neoantigen-reactivity displayed a high number of total T cells and intra-epithelial CD8$^+$ T cells, compared to the other MMR-p samples. Strikingly, the density of FoxP3$^+$ T cells in NIC3, NIC4, and NIC15 was higher than in any other sample. This observation is in line with the dominant role that TGF-β plays in these tumors as this growth factor is known to support the differentiation of regulatory T cells.

To determine whether CMS4 tumors displayed additional immune features that distinguish them from other MMR-p CRC, we investigated the expression of 78 immune-related genes (Additional file 3: Table S3) across CMS subtypes in the TCGA CRC dataset. Interestingly, an overall analysis placed the CMS4 group in between the CMS1 and CMS2/3 subtypes suggesting that immune features are more prominent in CMS4 tumors a s compared to other MMR-p CRC. Twelve genes were determined to be upregulated in the CSM4 subtype when compared to the CMS2/3 group, including *TGFB1*, in line with the most prominent biological feature of the former subtype. In addition, genes encoding important molecules involved in immune cell trafficking (*CXCL9* and *CXCL10*) and cellular adhesion (*ICAM1/CD54*, *ITGB2/CD18*, and *SELP*), HLA class II genes, the T cell checkpoint gene *HAVCR2* (TIM-3), *TNFSF4* (OX40L), as well as *PDCD1LG2* (PD-L2) were all shown to be upregulated in the CMS4 subtype in comparison to the CMS2/3 group (Figure 4C). Most of these genes were also shown to have increased expression in the CMS4 samples of the Leiden cohort in comparison to the CMS2/3 samples, albeit the lower number of samples (Figure 4D). The expression of the CXCL9 and CXCL10 chemokines, together with HLA

class II, OX40L, and PD-L2 are suggestive of the presence of antigen presenting cells in the microenvironment while TIM-3 expression may reflect an activated/dysfunctional phenotype of tumor-infiltrating T cells. Of note, the expression of TIM-3, OX40 ligand and PD-L2 were previously shown to be stimulated by TGF-β[48-50]. Altogether, we have found evidence that immune-related gene expression signatures are able to distinguish CRC of the CMS4 subtype from other MMR-p CRC.

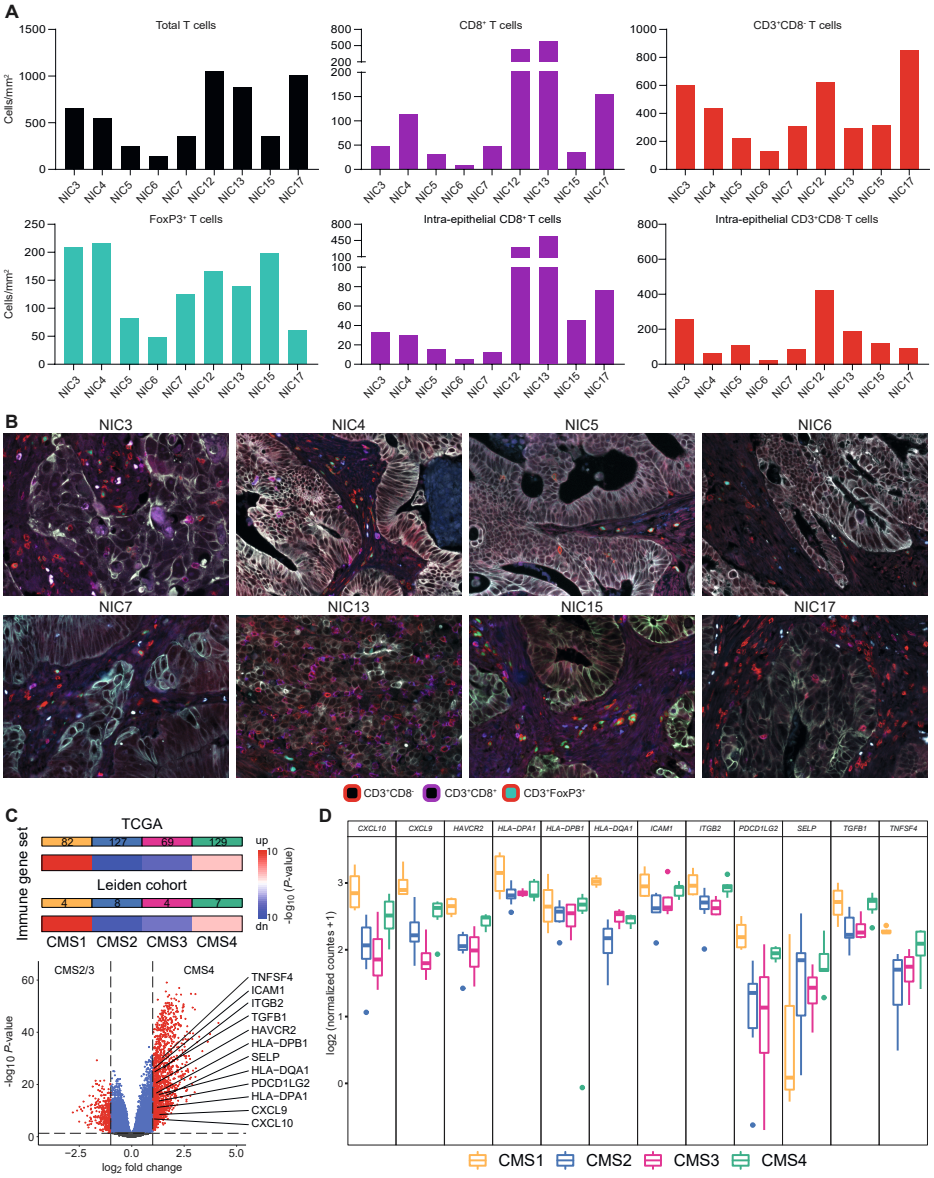

Figure 4 | *Immune infiltration and differentially expressed genes between NIC samples and CMS subtypes. (A) Quantitative analysis of immune cell infiltration by multispectral fluorescent imaging. Number of cells was counted per mm² of tissue (total) and epithelium (intra-epithelial). (B) Representative tissue sections demonstrating variable infiltration of immune cells in MMR-p (NIC3-7) and MMR-d tumors (NIC13). (C) Heatmaps showing the relative expression of immune regulatory genes for the CRC TCGA dataset and the Leiden cohort. Color saturation indicates the statistical significance; red and blue indicate the direction of change. Volcano plot shows differentially expressed genes between CMS2/3 (left) and CMS4 (right) samples. Statistically significant expressed genes from the immune gene set are depicted. (D) Box plot representing the gene expression per CMS subtype in the Leiden cohort of the differentially expressed immune genes determined in (C).*

DISCUSSION

The success of checkpoint blockade immunotherapies in patients diagnosed with cancers with high mutation burden[3,4,8-11] may emphasize the notion that tumors presenting few mutations are not amenable to immunotherapeutic strategies[3]. Here, we demonstrated that neoantigen-directed T cell responses occur naturally in CRC with low mutation burden. Specifically, we have detected responses against more than one neoantigen in three CRC cases that carried less than fifty transcribed, non-synonymous mutations. Interestingly, these cases belonged to the CMS4 molecular subtype, associated with a TGF-β-driven transcriptional signature and worse clinical outcome[12,13]. Although these results are derived from a small cohort and thus do not exclude the possibility to detect neoantigen-specific responses in CMS2 and CMS3, it proposes TGF-β as an interesting therapeutic target to augment immune responses in patients diagnosed with CMS4 cancers. TGF-β itself might be responsible for keeping the anti-tumor activity of neoantigen-specific T cells at bay in those patients. TGF-β is known to promote the differentiation of $CD4^+$ T cells into regulatory T cells (Tregs)[51], which is in line with the higher number of $CD3^+FoxP3^+$ cells that were observed in the CMS4 cases infiltrated by neoantigen-specific T cells. In addition, the increased number of intra-epithelial $CD8^+$ T cells in these MMR-p tumors may also relate to a TGF-β transcriptional signature, since TGF-β is known to regulate tissue residency of $CD8^+$ T cells by inducing the expression of integrins like αE (CD103) and α1, as well as CD69[52]. On the other hand, TGF-β can affect T cell populations by inhibiting IL-2 dependent proliferation[53] and their cytotoxic activity, which could impair the activity of neoantigen-reactive TIL *in vivo*[54-56]. In support of this, Tauriello and colleagues have shown that the therapeutic targeting of TGF-β, in CRC models reminiscent of the CMS4 subtype, unleashes the capacity of the adaptive immune system to eradicate tumors[57]. It is likely that this suppressive environment is lost during the extraction and culturing of neoantigen-reactive T cells, thereby allowing their detection in *in vitro* systems. The relevance of TGF-β as immune suppressor has also been demonstrated in a therapeutic setting in humans: TGF-β signaling activation in tumors was associated with a lack of response upon anti-PD-L1 treatment in urothelial cancer patients[58]. Currently, several initiatives are ongoing to augment responses to immunotherapeutic interventions by concomitantly targeting the TGF-β pathway[59,60].

Seminal work by Tran and colleagues demonstrated the feasibility of detecting neoantigen-directed T cell reactivity by TIL in gastrointestinal tumors, including CRC with moderate mutation burden (58 to 155 transcribed non-synonymous mutations)[61]. Moreover, the significant potential of neoantigen-specific T cells as therapeutic vectors in CRC has been highlighted by the successful treatment of a metastatic CRC patient by autologous cell transfer of a KRAS-mutant-reactive polyclonal T cell population[62]. Typically, the detection rate of neoantigen-specific T cell responses has been reported to range between 1 and 4% of the tested putative neoantigens[39,61]. Therefore, *a priori*, it was unlikely that neoantigen-specific T cell responses could be detected in CRC with low mutation burden

(below 50) like the ones reported in this work. Differences in methodological approaches, especially the use of RNA expression as a filter for variants to be screened, may explain such discrepancies although a greater number of research efforts are required for defining a range of detection of neoantigen-specific T cell reactivity across cancer types. Just recently, another research group demonstrated the existence of neoantigen-reactive T cells in various metastasis of MMR-p gastrointestinal tumors, including CRC[45]. These data combined with ours show that neoantigen-specific T cells reside in both the primary tumor as well as metastases of CRC. Interestingly, it is known that the CMS4 subtype is overrepresented in CRC metastatic disease[63] which is in line with our observations and the fact that Parkhurst and colleagues were able to demonstrate neoantigen-specific T cell responses in the majority of tumors analyzed.

Neoantigen-specific T cell responses have also been described in other tumor types with moderate to low mutation burden like ovarian cancer[64]. Moreover, personalized vaccination strategies, consisting of autologous dendritic cells pulsed with tumor lysate, prolonged the survival of ovarian cancer patients as therapeutic responses and were shown to be largely driven against cancer neoantigens[65]. Glioblastoma is another cancer type that is traditionally viewed as non-immunogenic due to the low number of mutations that occur in this disease. Remarkably, vaccination approaches with peptides corresponding to cancer neoantigens, in a personalized setting, were shown to promote tumor-specific immune reactions in glioblastoma patients[66,67]. Finally, a metastatic cholangiocarcinoma patient experienced disease regression and stabilization after therapeutic administration of T cell products generated from neoantigen-reactive $CD4^+$ T cells that recognized one neoantigen out of 26 transcribed mutations detected in the tumor tissue[68]. The detection of neoantigen-specific T cell responses and the success of some neoantigen-targeting therapeutic approaches are highly supportive of the notion that a broader proportion of cancer patients diagnosed with different tumor types may benefit from immunotherapeutic strategies, albeit personalized approaches will be required in those solid tumors which harbor mainly neoantigens derived from passenger genes and are thus heterogenic.

While checkpoint blockade therapies are currently ineffective in MMR-p CRC, the demonstration that neoantigen-reactive T cells infiltrate these tumors supports the development of alternative immunotherapeutic approaches that could include vaccination with biomolecules corresponding to immunogenic neoantigens or adoptive cell transfer of cancer-reactive T cells. To date, most adoptive T cell transfer therapy protocols are based on the non-controlled enrichment of heterogeneous mixtures of cancer-reactive and bystander T cells that may generate therapeutic products with suboptimal anti-cancer activity. The observation that neoantigen-reactive T cells can be identified by a specific phenotype, namely through co-expression of CD39 and CD103, can support their specific enrichment for downstream cellular therapies that can include cloning of the T cell receptors on non-exhausted donor T cells[17,40,47]. Here, we show that neoantigen reactivity can be attributed to this $CD39^+CD103^+$ $CD8^+$ T cell subset but additional investigations

are ongoing to confirm our observation. Additionally, the possibility to enrich for neoantigen-reactive $CD4^+$ T cell populations requires further exploration.

When T cells fail to infiltrate or persist in cancer tissues, vaccination approaches making use of biomolecules corresponding to neoantigens might be more suitable so that priming and mobilization of neoantigen-specific T cells can occur. The adoption of this strategy may be particularly suitable for the treatment of patients with MMR-p tumors, since: 1) the low neoantigen abundance allows the functional testing or therapeutic exploitation of the majority of cancer neoantigens in each patient with limited dependency on prediction algorithms and 2) these tumors are less frequently affected by immune evasion events such as defects in antigen presentation[41]. Independently of the immunotherapeutic approaches of choice, it is likely that concurrent strategies are required to provide inflammatory signals or breakdown of immune suppressive barriers for these patients. Among these, the complementary use of chemo- and radiotherapy as well as the employment of oncolytic viruses are promising approaches for the support of immunotherapies[69]. Further, and as demonstrated here, the immune infiltrate of CMS4 tumors comprises both tumor-reactive and immune suppressive cells, resulting in a strong rationale for blocking the TGF-β pathway in tumors that exhibit features of TGF-β activation in their microenvironment to unleash pre-existing T cell reactivity.

CONCLUSIONS

Taken together, our data demonstrate that autologous neoantigen-specific immune responses are present in patients diagnosed with MMR-p CRC of the CMS4 subtype. These findings support the adoption of specific immunotherapeutic strategies that deliver solutions for this patient group which may include neoantigen-based vaccines or enrichment of neoantigen-specific T cells for T cell therapies. The presence of neoantigen-reactive T cells in a milieu that is strongly associated with TGF-β activation also supports combinatorial strategies aimed at tackling this immune suppressive pathway.

COMPETING INTERESTS

T. Duhen and A.D. Weinberg disclose that they have submitted a patent regarding therapeutic and diagnostic use of the $CD39^+CD103^+$ $CD8^+$ T cells in cancer patients. The remaining authors declare that they have no competing interests.

FUNDING

This work was supported by the KWF Bas Mulder Award UL (2015-7664), the ZonMw Veni grant (016.176.I44), the Fight Colorectal Cancer-Michael's Mission-AACR Fellowship in Young Onset, Late-Stage Colorectal Cancer Research 2015 (15-40-1645-DEMI). J. van den Bulk was supported by an LUMC PhD fellowship.

ACKNOWLEDGEMENTS

We thank MG Kallenberg-Lantrua and residents of the department of Pathology for her help with collection of patient material and the reviewers of this manuscript for their invaluable input.

APPENDIX

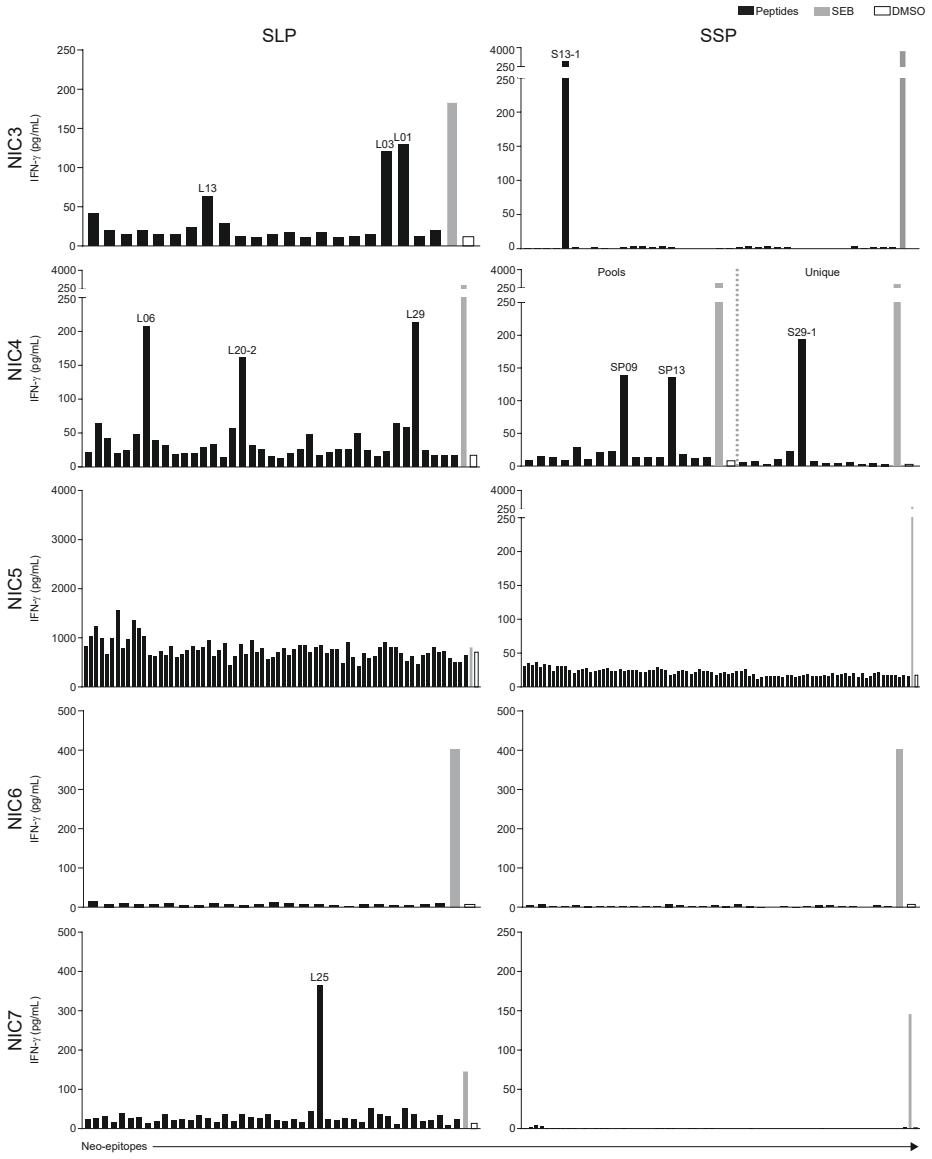

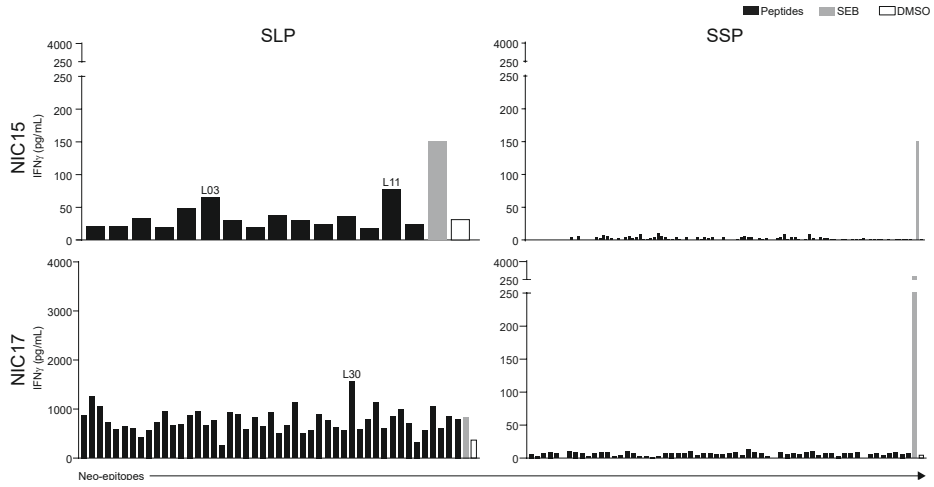

Figure S1 *| Neoantigen-specific reactivity screen of the expanded TIL from NIC3-7, NIC15 and NIC17 towards SLPs and SSPs. IFN-γ production (y-axis) is shown for each neo-epitope that was tested (black bars, x-axis) and the positive (grey bar) and negative control (white bar). Peptide IDs are included for neo-epitope responses that were judged positive and selected for validation. SSPs and SLPs with the same ID number correspond to the same mutation per patient.*

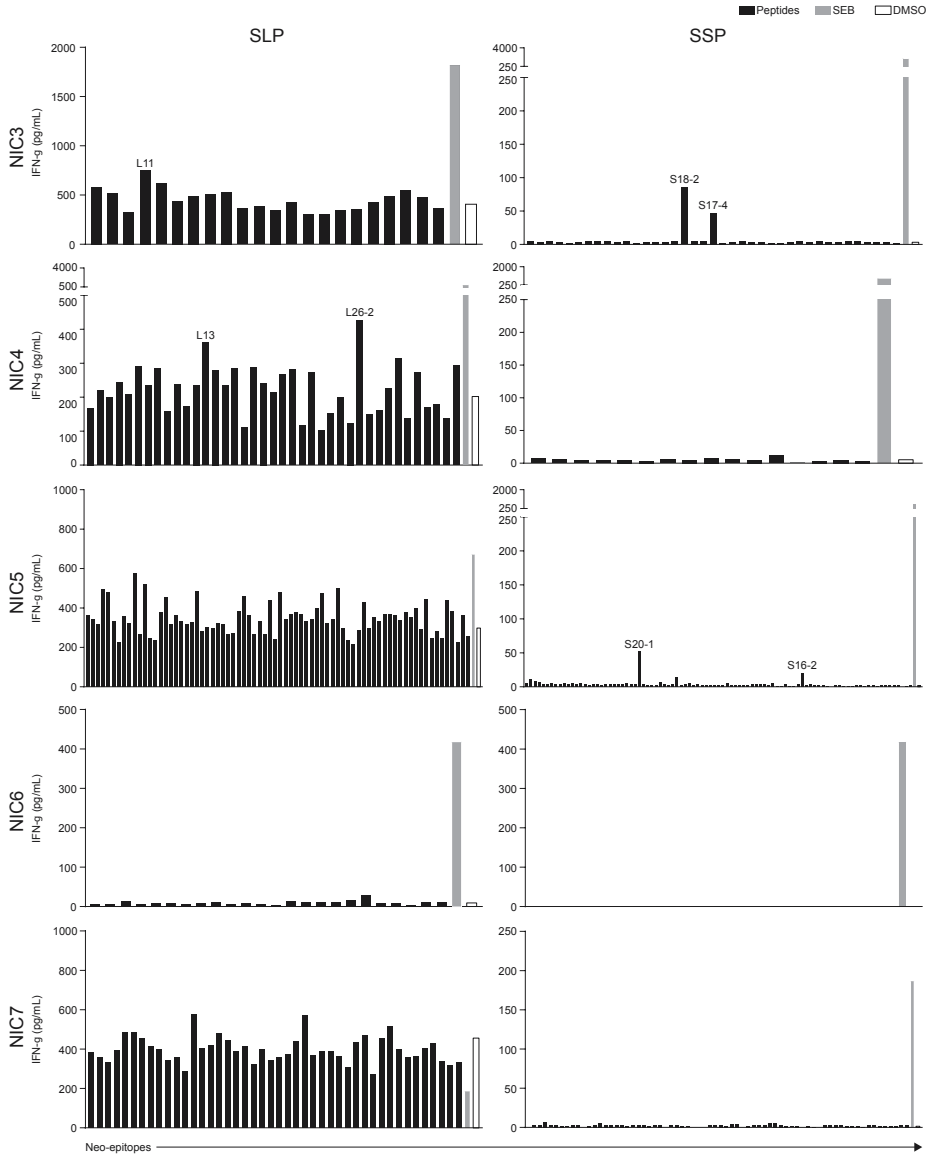

Figure S2 | *Neoantigen-specific reactivity screen of the PBL from NIC3-7 towards SLPs and SSPs. IFN-γ production (y-axis) is shown for each neo-epitope that was tested (black bars, x-axis) and the positive (grey bar) and negative control (white bar). Peptide IDs are included for neo-epitope responses that were judged positive and selected for validation. SSPs and SLPs with the same ID number correspond to the same mutation per patient.*

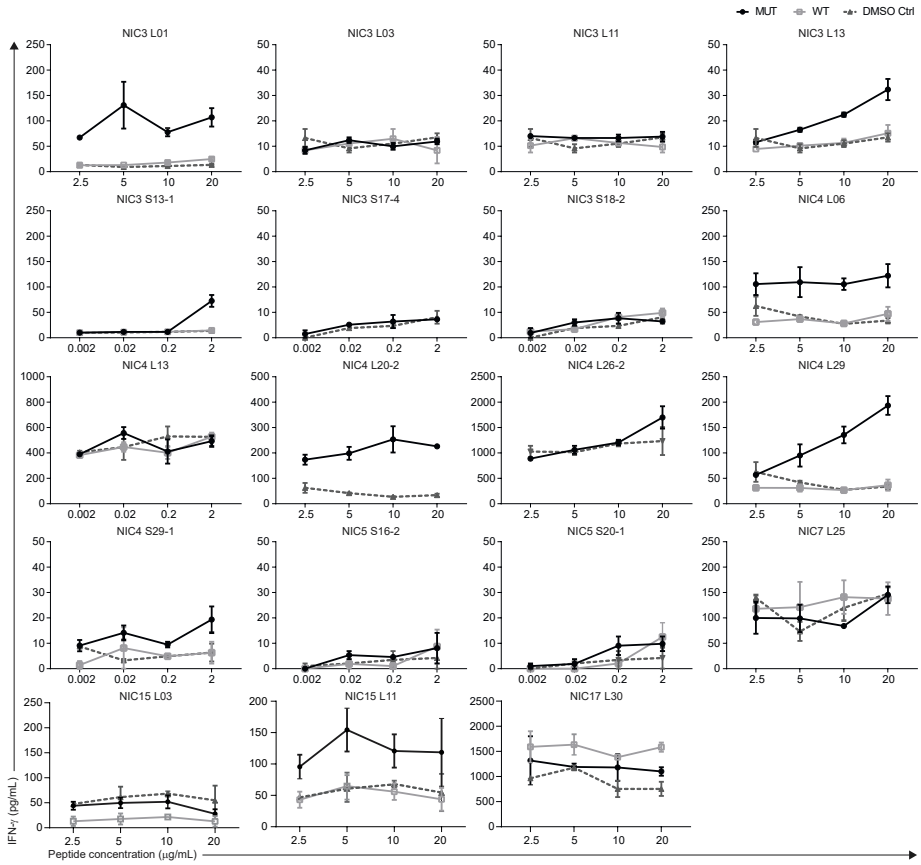

Figure S3 | *Validation of the neoantigen-specific responses detected in the first screen. IFN-γ production of TIL and PBL from NIC3-7, NIC15 and NIC17 was measurement upon stimulation with mutant (black) and wild type (grey) HPLC peptides, and a DMSO control (dashed), at different peptide concentrations. The mean ± standard deviation of the biological duplicates in the same experiment are depicted.*

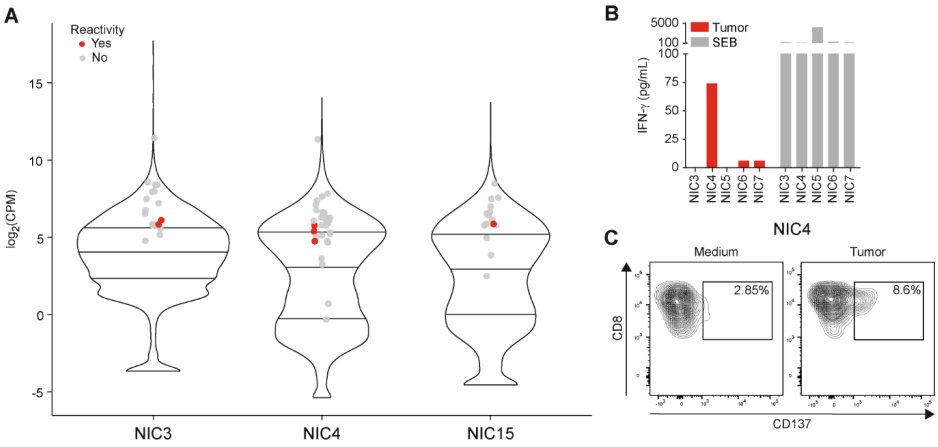

Figure S4 | *A) RNA expression of genes encoding somatic mutations (dots) in relation to overall gene expression level in NIC3, NIC4, and NIC15. Red dots highlight the genes to which neoantigen-specific T cell responses were observed. B) Measurement of IFN-γ production upon co-culture of TIL with autologous tumor material (red) or SEB (positive control, grey). C) Flow cytometric analysis of CD8⁺ TIL cultures derived from NIC4 shows an increase of CD137 expression upon co-culture with autologous tumor material compared to the medium control. The percentage in the gates refer to the CD137-positive fraction within the CD8⁺ subset.*

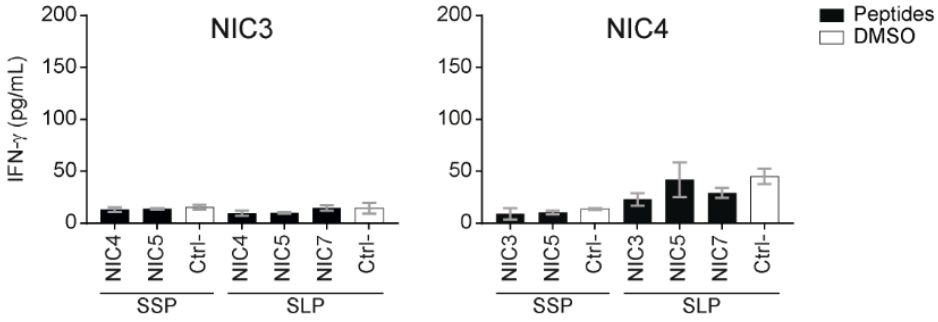

Figure S5 | *Cross-reactivity of the T cells. TIL (black) were tested towards peptide pools of other patients including SLP loaded on EBV-LCL and SSP. Medium with DMSO (white) with or without EBV-LCL were taken along as negative control for the SLP and SSP, respectively. This cross-reactivity setting shows the patient-specific nature of neoantigen reactivity. The mean ± standard deviation of the biological duplicates in the same experiment are depicted.*

Table S1 | HLA class I genotypes determined by exome and transcriptome sequencing.

Patient ID	HLA-A		HLA-B		HLA-C	
NIC3	A*02.01	A*33.03	B*18.01	B*27.02	C*02.02	C*07.01
NIC4	A*02.01	A*03.01	B*08.01	B*44.03	C*04.01	C*07.02
NIC5	A*02.01	A*32.01	B*07.02	B*15.01	C*03.04	C*07.02
NIC6	A*24.02	A*24.02	B*14.02	B*55.01	C*03.03	C*08.02
NIC7	A*01.01	A*32.01	B*40.01	B*51.01	C*03.04	C*15.02
NIC12	A*01:01	A*32:01	B*08:01	B*27:05	C*02:02	C*07:01
NIC13	A*02:01	A*11:01	B*35:01	B*44:02	C*04:01	C*05:01
NIC15	A*11:01	A*24:02	B*44:02	B*51:01	C*05:01	C*15:02
NIC17	A*01:01	A*24:02	B*08:01	B*35:03	C*04:01	C*07:01

Table S2 | Mutant peptide sequences that were investigated for T cell reactivity.

Patient ID	Mutational position	Mutation type	Gene	SLP ID	Long sequences	SSP ID	Short sequences	ALT_ DNA
NIC3	chr11_12473817_C/G	Missense	PARVA	L01	NLPLSPIPFELDREDTMLEENEVRT	S01-1	FELDREDTM	0,11
						S01-2	SPIPFELDR	
NIC3	chr14_77597202_T/A	Missense	SPTLC2	L02	RYWRIEKCHHATVREEQKDFVSLYQ			0,08
NIC3	chr15_85693368_T/A	Missense	AKAP13	L03	KEKDKKTVNGHTYSSIPVVGPISCS			0,07
NIC3	chr16_69150545_C/A	Missense	UTP4	L04	ADVQSIAVADQEESFVVGTAEGTVF	S04-1	EESFVVGTA	0,12
						S04-2	AVADQEESF	
						S04-3	EESFVVGT	
NIC3	chr17_63837477_G/T	Missense	SMARCD2	L05	TMMDPFRKRLLVHQAQPPMPAQRRG	S05-1	FRKRLLVHQ	0,15
						S05-2	KRLLVHQAQPPM	
						S05-3	LVHQAQPPM	
NIC3	chr17_75834981_G/A	Missense	UNC13D	L06	DLSTCFAQISHTVRQLDWPDPEEAF	S06-1	FAQISHTVR	0,11
						S06-2	QISHTVRQL	
NIC3	chr19_15401395_G/A	Missense	AKAP8L	L07	RAQGWARDARSGWPMASGYGRMWED	S07-1	ARSGWPMASGY	0,21
						S07-2	ARSGWPMAS	
						S07-3	ARDARSGW	
						S07-4	SGWPMASGY	
NIC3	chr19_19638174_C/G	Missense	GMIP	L08	PSKQQERRRRSRDEAQAKAQEAEAL	S08-1	DEAQAKAQ	0,11
						S08-2	RRRSRDEAQ	
NIC3	chr2_127630830_A/C	Missense	MYO7B	L10	SPEKRKLAAQEGPFTEPRPEEPPKE			0,13
NIC3	chr2_86466578_C/G	Missense	KDM3A	L11	PKTNTDQENRLECVPQALTGLPKEC	S11-1	NRLECVPQAL	0,11
						S11-2	LECVPQAL	
						S11-3	NRLECVPQA	
NIC3	chr20_63673995_C/T	Missense	RTEL1-TNFRSF6B	L12	SASFDLTPHDLALGLDVIDQVLEEQ	S12-1	ALGLDVIDQV	0,09
						S12-2	FDLTPHDLAL	
NIC3	chr5_151790961_G/A	Missense	G3BP1	L13	NCHTKIRHVDAHTTLNDGVVVQVMG	S13-1	IRHVDAHTTL	0,11

Table S2 | Mutant peptide sequences that were investigated for T cell reactivity. *(continued)*

Patient ID	Mutational position	Mutation type	Gene	SLP ID	Long sequences	SSP ID	Short sequences	ALT_ DNA
						S13-2	RHVDAHTTL	
NIC3	chr6_106512921_G/T	Missense	AIM1	L15	PLPNHFNGRAEGCRSRKLGRAAGAP	S15-1	AEGCRSRKL	0,06
						S15-2	HFNGRAEGCR	
						S15-3	HFNGRAEGCRSR	
NIC3	chr6_106512933_G/A	Missense	AIM1	L16	HFNGRAEGCRSRKLGRAAGAPGASD			0,06
NIC3	chr7_131443658_ GAGGACATCCAGTCTCGAAT/G	Frameshift	MKLN1	L17-1	LREDSCNAGPEDTACYSTQKIVAYM	S17-1	KIVAYMYLV	0,09
				L17-2	EDTACYSTQKIVAYMYLVASDQRPI	S17-2	MYLVASDQR	
						S17-3	YSTQKIVAY	
						S17-4	STQKIVAYM	
NIC3	chr7_139079778_A/G	Missense	ZC3HAV1	L18	VFSPTLPAARSSPGSLQTPEAVTTR	S18-1	ARSSPGSLQ	0,12
						S18-2	AARSSPGSL	
NIC3	chr8_144842234_C/A	Missense	ZNF7	L19	CKECGKAFSQSSNLAQHQRMHTGEK	S19-1	SSNLAQHQR	0,14
						S19-2	KAFSQSSNL	
						S19-3	FSWSNTTLL	
NIC3	chrM_11931_T/C	Missense	MT-ND4	L20	LSVLVTTFSWSNTTLLLTGLNMLVT	S20	YLLKVCERI	0,22
NIC3	chrX_80793730_T/C	Missense	BRWD3	L21	ANAHIPPDYLLKVCERIGPLLDKEI	S21	DYLLKVCER	0,08
NIC4	chr1_11950386_G/A	Missense	PLOD1	L01	ADSYDVLFASGPQELLKKFRQARSQ	S01	VLFASGPRELLK	0,53
NIC4	chr11_14818305_G/A	Missense	PDE3B	L02	FPDTADFLNKPSIILQRSLGNAPNT	S02	FLNKPSIIL	0,16
NIC4	chr11_74374521_C/T	Missense	PGM2L1	L03	ENLLRNGMNKELQDRLCCRMTFGTA			0,27
NIC4	chr11_86446352_G/A	Missense	ME3	L04	PGVALGVIAGGIWHIPDEIFLLTAE	S04	VIAGGIWHI	0,25
NIC4	chr12_25245347_C/T	Missense	KRAS	L05	YKLVVVGAGDVGKSALTIQLIQ			0,30
NIC4	chr14_58223625_G/A	Missense	ACTR10	L06	SVPEGVLEDIKAHTCFVSDLKRGLK	S06-1	DIKAHTCFV	0,15
						S06-2	LEDIKAHTCF	
NIC4	chr14_73276592_C/T	Missense	NUMB	L07	PSPTNPFSSDLQKTFKIEL	S07	FSSDLQKTF	0,31
NIC4	chr14_73276674_C/G	Missense	NUMB	L08	TGTCPVDPFEAQCAALENKSKQRTN	S08	PFEAQCAAL	0,28
NIC4	chr14_80792789_C/A	Missense	CEP128	L09	KLERALEKQSETFDELTGKNNQILK	S09-1	SETFDELTGK	0,20

Table S2 | Mutant peptide sequences that were investigated for T cell reactivity. *(continued)*

Patient ID	Mutational position	Mutation type	Gene	SLP ID	Long sequences	SSP ID	Short sequences	ALT_ DNA
						S09-2	TFDELTGKN	
NIC4	chr16_28830704_G/C	Missense	ATXN2L	L10	GVRCSSSRGGRPALSSLPPRGPHHL			0,26
NIC4	chr17_42787309_A/G	Missense	WNK4	L11	EMVALGLVCEADCQPVARAVRERVA	S11	CEADCQPVA	0,49
NIC4	chr17_44190551_G/A	Missense	TMUB2	L12	GQESQMKLIYQGHLLQDPARTLRSL	S12-1	KLIYQGHLL	0,16
						S12-2	LIYQGHLLQDPAR	
						S12-3	QMKLIYQGHL	
NIC4	chr17_63420571_G/A	Missense	TANC2	L13	PPPVGGQGKEYPNPPPSPLRRGPQY	S13	YPNPPPSPL	0,47
NIC4	chr17_7674221_G/A	Missense	TP53	L14	YMCNSSCMGGMNWRPILTIITLEDSSG	S14-1	CMGGMNWRPI	0,40
						S14-2	GMNWRPILTI	
						S14-3	MGGMNWRPIL	
NIC4	chr19_10555328_CCTT/C	Inframe deletion	KRI1	L15	FGLSTEEILAADDELNRWCSLKKTCM	S15	EEILAADDELNRW	0,12
NIC4	chr19_1093973_G/A	Missense	POLR2E	L16	QFGDKPSEGRPRCTDLTVLVAHNDD	S16	EGRPRCTDL	0,22
NIC4	chr19_13074002_C/A	Missense	NFIX	L17	YYNINQVTLGRRYITSPPSTSTTKR	S17-1	TLGRRYITS	0,36
						S17-2	LGRRYITSP	
						S17-3	NQVTLGRRY	
NIC4	chr2_219615172_C/T	Missense	STK11IP	L18	TLFLLDEDAAGSLAEPSPPAASGEA	S18-1	SLAEPSPPA	0,37
						S18-2	FLLDEDAAGSL	
						S18-3	DEDAAGSLA	
NIC4	chr2_74889415_G/A	Missense	HK2	L19	AGMAAVVDRIRENHGLDALKVTVGV	S19-1	RIRENHGLDALK	0,07
						S19-2	RENHGLDAL	
NIC4	chr20_57378098_A/G	Stop loss	RAE1	L20-1	NAAEELKPRNKKWWLETLAQPELFL	S20-1	KPRNKKWWL	0,13
				L20-2	WWLETLAQPELFLSTLPHLCTNLGP	S20-2	WRKRCHCSA	
				L20-3	LSTLPHLCTNLGPSLVGLSAMDMDF	S20-3	WRKRCHCSAA	
				L20-4	PSLVGLSAMDMDFNPWRKRCHCSAA	S20-4	EELKPRNKKW	
				L20-5	FNPWRKRCHCSAAESPGVRGDLPSL	S20-5	LFLSTLPHL	
				L20-6	SAAESPGVRGDLPSLHSTACCRVFL			

Table S2 | Mutant peptide sequences that were investigated for T cell reactivity. *(continued)*

Patient ID	Mutational position	Mutation type	Gene	SLP ID	Long sequences	SSP ID	Short sequences	ALT_ DNA
NIC4	chr3_11259275_G/A	Missense	HRH1	L21	SLSVADLIVGAVIMPMNILYLLMSK			0,21
NIC4	chr3_192144025_T/G	Missense	FGF12	L22	SGTPTMNGGKVVTQDST			0,27
NIC4	chr3_37298887_G/A	Missense	GOLGA4	L23	VKTLETLQQRVKHQENLLKRCKETI	S23	RVKHQENLLK	0,12
NIC4	chr4_143185536_C/T	Missense	USP38	L24	LKRVIVRKVVESVEHWLDEAQCEAM			0,39
NIC4	chr5_103028911_T/A	Missense	PAM	L25	GRFRGKGSGGLNHGNFFASRKGYSR	S25	GLNHGNFFA	0,11
NIC4	chr5_112838150_GGA/G	Frameshift	APC	L26-1	SSRSEKDRSLERTRNWSRQLPSSNR	S26-1	YLSGRQKFWV	0,11
				L26-2	TRNWSRQLPSSNRKSRNFFKARFAD	S26-2	HSYLSGRQK	
				L26-3	RKSRNFFKARFADLHHCSPDCQSHG	S26-3	FFKARFADL	
				L26-4	DLHHCSPDCQSHGRSVSHSYLSGRQ	S26-4	LERTRNWSR	
				L26-5	PDCQSHGRSVSHSYLSGRQKFWVYH	S26-5	SYLSGRQKF	
						S26-6	SRNFFKARF	
						S26-7	SRSEKDRSL	
						S26-8	RTRNWSRQL	
NIC4	chr7_94400200_C/T	Missense	COL1A2	L27	PAGDRGPRGERGLPGPPGRDGEDGP			0,18
NIC4	chr8_142613268_C/T	Missense	ARC	L28	QYVVGTLQPKLKHFLRHPLPKTLEQ			0,23
NIC4	chr8_93923083_C/T	Missense	PDP1	L29	PKSEAKSVVKQDWLLGLLMPFRAFG	S29-1	SEAKSVVKQDW	0,45
						S29-2	SEAKSVVKQDWL	
						S29-3	KQDWLLGLL	
NIC4	chrX_1593799_C/T	Missense	AKAP17A	L30	IKLSGFSDILKVCAAEFKIDFPTRH	S30	ILKVCAAEFK	0,15
NIC5	chr1_171584051_A/C	Missense	PRRC2C	L01	TAIHNFPTVQHQALAKAQSGLAFQQ	S01	FPTVQHQAL	0,20
NIC5	chr1_207767803_C/T	Missense	CD46	L02-1	LSHSVSTSSTTKFPASSASGPRPTY	S02-1	SVSTSSTTKF	0,40
				L02-2	KCLKVSTSSTTKFPASSASGPRPTY	S02-2	KVSTSSTTKF	
				L02-3	KCLKVSTSSTTKFPASSASGYPKPE	S02-3	FPASSASGY	
NIC5	chr1_209783196_G/C	Missense	C1orf74	L03	LKALVAEIITHLEGLQRDLSLAVSY			0,25
NIC5	chr1_46270754_C/T	Missense	RAD54L	L04	AASEADRQLGEEWLRELTSIVNRCL	S04	WLRELTSIV	0,81
NIC5	chr1_90027699_T/G	Stop lost	ZNF326	L05-1	EELEEETAKEEPADFPVEQPEENEI			0,44
				L05-2	PADFPVEQPEENEI			

Table S2 | Mutant peptide sequences that were investigated for T cell reactivity. *(continued)*

Patient ID	Mutational position	Mutation type	Gene	SLP ID	Long sequences	SSP ID	Short sequences	ALT_ DNA
NIC5	chr10_114575476_T/A	Missense	ABLIM1	L06	TRCHGCGEFVEGVVVTALGKTYHPN	S06	VVVTALGKTY	0,07
NIC5	chr11_66020856_T/A	Missense	CATSPER1	L08	IFTTIFTLFTLLSLDDWSLIYMDSR	S08-1	SLDDWSLIYM	0,23
						S08-2	TLLSLDDWSL	
						S08-3	LLSLDDWSL	
NIC5	chr11_67999580_C/T	Missense	UNC93B1	L09	NYWERYYTLVPSTVALGMAIVPLWA	S09-1	TLVPSTVAL	0,24
						S09-2	YYTLVPSTV	
						S09-3	STVALGMAI	
						S09-4	YYTLVPSTVAL	
NIC5	chr11_95783089_T/A	Missense	FAM76B	L10-1	HPKHHHHHHHHHHLRHSSSHHKISNL	S10-1	HHHHHHHHL	0,11
				L10-2	RKTSIIQNIITTIITITFVTAVAIT	S10-2	ITFVTAVAI	
						S10-3	ITTIITITF	
NIC5	chr13_45525021_A/G	Missense	COG3	L11-1	LKTMASQGGPKYALSQQPWAQPAKV	S11-1	RPQVCSLTAAL	0,08
				L11-2	VKNNGQSGRPQVCSLTAALGTTSKG	S11-2	RPQVCSLTA	
						S11-3	RPQVCSLTAA	
						S11-4	RPQVCSLTAALG	
						S11-5	GRPQVCSLTAAL	
NIC5	chr13_98809435_G/A	Missense	DOCK9	L12	FERLAHLYDTLHWAYSKVTEVMHSG	S12-1	HLYDTLHWA	0,29
						S12-2	LYDTLHWAY	
NIC5	chr14_103135969_G/A	Missense	TNFAIP2	L13	VSTASIRRHIQVAPQPLQAGPAMGP	S13-1	QPLQAGPAM	0,76
						S13-2	APQPLQAGPAM	
NIC5	chr14_64065516_G/A	Missense	SYNE2	L14	RQILRLLRLRCTKNDGICLLKIVSA	S14	RLLRLRCTK	0,83
NIC5	chr15_41669457_A/T	Missense	MGA	L15	FYKLKLTNNTLDLEGHIILHSMHRY	S15-1	TLDLEGHIIL	0,48
						S15-2	KLTNNTLDL	
NIC5	chr16_346835_G/A	Missense	AXIN1	L16	IKGETSTATPRRLDLDLGYEPEGSA	S16-1	TPRRLDLDL	0,09
						S16-2	ATPRRLDLDL	
						S16-3	RRLDLDLGY	
NIC5	chr16_88631239_G/T	Missense	ZC3H18	L17	ASTLSRREELLKHLKAVEDAIARKR	S17	RREELLKHL	0,06

Table S2 | Mutant peptide sequences that were investigated for T cell reactivity. *(continued)*

Patient ID	Mutational position	Mutation type	Gene	SLP ID	Long sequences	SSP ID	Short sequences	ALT_ DNA
NIC5	chr17_39725079_G/A	Missense	ERBB2	L19	AKGMSYLEDVRLIHRDLAARNVLVK	S19	SYLEDVRLI	0,44
NIC5	chr17_48860426_T/C	Missense	CALCOCO2	L20	TSDEGGARQNPGPAYGNPYSGIQES	S20-1	RQNPGPAY	0,08
						S20-2	ARQNPGPAY	
NIC5	chr17_58357951_G/A	Missense	RNF43	L21	QVTRSNSAAPSGWLSNPQCPRALPE	S21	APSGWLSNPQ	0,20
NIC5	chr17_7673776_G/A	Missense	TP53	L22	FEVRVCACPGRDWRTEEENLRKKGE			0,73
NIC5	chr19_48441818_C/T	Missense	GRIN2D	L23	FIYDAAVLNYMACKDEGCKLVTIGS	S23	YMACKDEGCKLV	0,53
NIC5	chr19_49447035_G/C	Missense	PIH1D1	L24-1	LEAPDLLLAEVDVPKLDGALGLSLE	S24-1	LLAEVDVPKL	0,05
				L24-2	LEAPDLLLAEIDVPKLDGALGLSLE	S24-2	LLAEIDVPKL	
				L24-3	HLNLWLEAPDLLLAEIDVPKLTLQI	S24-3	LLAEIDVPKL	
				L24-4	LEAPDLLLAEIDVPKLINSHESKAA	S24-4	VPKLDGALGL	
						S24-5	VPKLDGAL	
						S24-6	VPKLDGALGLSL	
NIC5	chr19_55401666_G/A	Missense	UBE2S	L25	RLLLENYEEYAAWARLLTEIHGGAG	S25-1	EYAAWARLL	0,07
						S25-2	YEEYAAWARLL	
NIC5	chr2_110144543_C/G	Missense	NPHP1	L26	IPAKTYELFLNGATPYEKGIEVDPS	S26	ATPYEKGIEV	0,29
NIC5	chr2_127050828_C/A	Missense	BIN1	L27	GTVEGGSGAGRLYLPPGFMFKVQAQ	S27-1	LYLPPGFMF	0,06
						S27-2	YLPPGFMFKV	
						S27-3	YLPPGFMF	
						S27-4	RLYLPPGF	
						S27-5	LYLPPGFMFKV	
						S27-6	RLYLPPGFMFKV	
NIC5	chr2_127426153_G/A	Missense	PROC	L28	MEKKRSHLKRDTKDQEDQVDPRLID			0,05
NIC5	chr2_240462422_A/T	Missense	GPC1	L29	LFKQLHPQLLLPVDYLDCLGKQAEA	S29-1	QLLLPVDYL	0,09
						S29-2	LLPVDYLDCL	
						S29-3	LPVDYLDCL	
NIC5	chr2_240462422_A/T	Missense	GPC1	L29	LFKQLHPQLLLPVDYLDCLGKQAEA	S29-4	HPQLLLPVDYL	
						S29-5	QLHPQLLLPV	

Table S2 | Mutant peptide sequences that were investigated for T cell reactivity. *(continued)*

Patient ID	Mutational position	Mutation type	Gene	SLP ID	Long sequences	SSP ID	Short sequences	ALT_ DNA
						S29-6	HPQLLLPV	
NIC5	chr2_96298337_G/C	Missense	SNRNP200	L30	ERIMGKMEADPEVSKFLYQLHETEK	S30-1	MEADPEVSKF	0,11
						S30-2	IMGKMEADPEV	
						S30-3	RIMGKMEADPEV	
NIC5	chr20_18183172_C/T	Missense	KAT14	L31	TKPPKLQLLSQICSHLHRSDPHWTP			0,06
NIC5	chr20_46374418_C/T	Missense	ELMO2	L32	DTYIRIVLENSSQEDKHECPFGRSA	S32	SQEDKHECPF	0,07
NIC5	chr4_139370290_G/C	Missense	NAA15	L34	QRRAQKKAQIEEDKKNAEKEKQQRN			0,55
NIC5	chr4_148120260_C/T	Missense	NR3C2	L35-1	NLGERRCISLPCINYARGCTKSAFS	S35-1	KLCQGMHQI	0,07
				L35-2	FNEEKMHQSAMYKLCQGMHQISLQF	S35-2	AMYKLCQGM	
NIC5	chr5_112839398_AAT/A	Frameshift	APC	L36	CKVSSINQETIQTYCVEDTPMFFKM	S36-1	QTYCVEDTPM	0,40
						S36-2	TYCVEDTPM	
NIC5	chr5_112839906_AC/A	Frameshift	APC	L37-1	SPGQTMPPSRSKNLHHLLKQLKPSE	S37-1	KQLKPSEKY	0,42
				L37-2	KNLHHLLKQLKPSEKYLKIKHLLLK	S37-2	SRSKNLHHL	
				L37-3	KPSEKYLKIKHLLLKRERVDLSKLQ			
NIC5	chr5_138924582_G/A	Missense	CTNNA1	L38	IALQEKDVDGLDHTAGAIRGRAARV			0,45
NIC5	chr5_157809736_G/A	Missense	CLINT1	L39	WDEEWDKNKSAFLFSDKLGELSDKI	S39	FLFSDKLGEL	0,33
NIC5	chr6_105282511_C/G	Missense	PREP	L40	DFQCAAEYLIKERYTSPKRLTINGG	S40	ERYTSPKRL	0,04
NIC5	chr6_136356706_T/A	Missense	MAP7	L42	VGSPHVVTSHQSNVTVESTPDLEKQ	S42	TSHQSNVTV	0,20
NIC5	chr6_168078950_T/A	Missense	FRMD1	L43	CSQQEPTLGMDALASEHRDVLVLLP	S43-1	LASEHRDVL	0,09
						S43-2	ALASEHRDVLV	
						S43-3	QEPTLGMDAL	
						S43-4	EPTLGMDAL	
						S43-5	SQQEPTLGMDAL	
NIC5	chr7_76625578_T/TTTCTCC	Inframe insertion	POMZP3	L45	TVLSALKEKKKKEKRTVEEEDQIFL			0,16
NIC5	chr7_99454126_C/G	Missense	CPSF4	L46-1	AGNRGPRPLEQVSCYKCGEKGHYAN	S46-1	RSAVTSVAR	0,30
				L46-2	AGNRGPRPLEQVSCYKCCCLSLLFP	S46-2	RGPRPLEQVS	

Table S2 | Mutant peptide sequences that were investigated for T cell reactivity. *(continued)*

Patient ID	Mutational position	Mutation type	Gene	SLP ID	Long sequences	SSP ID	Short sequences	ALT_ DNA
				L46-3	RATGDPGHWSRSAVTSVARKDTTPT	S46-3	DPGHWSRSAV	
						S46-4	RPLEQVSCY	
NIC5	chr8_100153299_G/A	Missense	POLR2K	L47	IRCRECGYRIMYKKRTKRLVIFDAR	S47	KRTKRLVIF	0,39
NIC5	chr8_37899408_C/A	Missense	RAB11FIP1	L48	MSLMVSAGRGLWAVWSPTHVQVTVL	S48	MVSAGRGLW	0,15
NIC5	chr8_73673126_G/C	Missense	STAU2	L49-1	KPFPNYRANYNFGGMYNQRYHCPVP	S49	RANYNFGGMY	0,43
				L49-2	KPFPNYRANYNFGGMYNQRWQHLNG			
				L49-3	YRPLDPKPFPNYRANYNFGGMYNQR			
NIC5	chr9_114169425_A/G	Missense	COL27A1	L50	FHLAGSTPFPLLVGPPGPKGDCGLP			0,41
NIC5	chr9_134050430_G/T	Missense	BRD3	L51	VTSVPVPPAAAPTPPATPIVPVVPP	S51-1	APTPPATP	0,34
						S51-2	AAPTPPATPI	
						S51-3	APTPPATPIV	
NIC5	chr9_134690995_C/T	Missense	COL5A1	L52	DGITKTTGFCATWRSSKGPDVAYRV	S52	KTTGFCATW	0,42
NIC5	chr9_136946680_G/A	Missense	C8G	L53	QIFYFPKYGFCEAADQFHILDEVRR	S53	EAADQFHIL	0,50
NIC5	chr9_19378868_C/T	Missense	RPS6	L54	RISGGNDKQGFPIKQGVLTHGRVRL	S54	FPIKQGVL	0,07
NIC5	chrX_49065811_G/A	Missense	CCDC120	L55	SSFEGRSVPATPILTRGAGPQLCKP	S55-1	RSVPATPIL	0,17
						S55-2	TPILTRGAGPQL	
						S56	KRLVRGRRL	
NIC6	chr1_1495770_T/A	Missense	ATAD3B	L01	GLCPGPLSPRMSSGGGRPFCPPGHP	S01-1	MSSGGGRPF	0,30
						S01-2	GPLSPRMSS	
NIC6	chr11_57487147_T/A	Missense	SLC43A1	L02	LQSLISAVFALLLQPLFMAMVGPLK	S02-1	LLQPLFMAM	0,29
						S02-2	VFALLLQPLF	
NIC6	chr11_61726066_C/T	Missense	DAGLA	L03	SRRLKVFLCCTRMKDSQSDAYSEIA	S03-1	SRRKVDYIL	0,38
						S03-2	MKDSQSDAY	
NIC6	chr11_70087815_G/A	Missense	ANO1	L04	DAECKYGLYFRDSRRKVDYILVYHH			0,36
NIC6	chr1_21838948_C/T	Missense	HSPG2	L05	QWSRVGSSLPGRTTARNELLHFERA	S05	SSLPGRTTA	0,68
NIC6	chr12_25245347_C/T	Missense	KRAS	L06	MTEYKLVVVGAGDVGKSALTIQLIQ	S06	AGDVGKSAL	0,30
NIC6	chr1_226161618_C/T	Missense	ACBD3	L07	EERERLQKEEEKHRREEEERLRREE			0,36

Table S2 | Mutant peptide sequences that were investigated for T cell reactivity. *(continued)*

Patient ID	Mutational position	Mutation type	Gene	SLP ID	Long sequences	SSP ID	Short sequences	ALT_ DNA
NIC6	chr12_48693925_T/C	Missense	CCNT1	L08	YAYAAQNLLSHHGSHSSVILKMPIE	S08-1	SHHGSHSSV	0,14
						S08-2	VSVSTSHTI	
NIC6	chr12_52675336_TGCC/T	Inframe deletion	KRT1	L09	GGYRGGSGGGGGSSGGRGSGGGSSG			0,25
NIC6	chr12_52675593_ATGG/A	Inframe deletion	KRT1	L10	PNVSVSVSTSHTISGGGSRGGGGGG			0,27
NIC6	chr12_7149082_G/A	Missense	CLSTN3	L11	PQILLSGTAHFAHPAVDFEGTNGVP	S11-1	TAHFAHPAV	0,39
						S11-2	FAHPAVDFE	
NIC6	chr15_72774962_C/T	Missense	ADPGK	L12	SRNDLEEAFIHFIGKGAAAERFFSD	S12	HFIGKGAAAERF	0,45
NIC6	chr16_67285438_C/G	Missense	PLEKHG4	L13	GLRGQRAHLFGNVEKLRDFHCHFFL	S13	HLFGNVEKL	0,36
NIC6	chr17_7674885_C/T	Missense	TP53	L14	EYLDDRNTFRHSMVVPYEPPEVGSD	S14-1	DRNTFRHSM	0,64
						S14-2	DDRNTFRHSM	
NIC6	chr19_39878097_G/A	Missense	FCGBP	L15	QVSYDWNWRVDVMLPSSYHGAVCGL	S15	DWNWRVDVM	0,14
NIC6	chr19_45364293_G/A	Missense	ERCC2	L16	NVCIDSMSVNLTCRTLDRCQGNLET			0,39
NIC6	chr20_50891938_TCTC/T	Inframe deletion	ADNP	L17	LKVIPEDASESEKLDQKEDGSKYET			0,20
NIC6	chr3_194425432_T/C	Missense	ATP13A3	L18	LDEHNIQNYENTAVFFISSFQYLIV	S18-1	NYENTAVFF	0,34
						S18-2	NYENTAVFFI	
NIC6	chr4_185399669_ AATAAAAGCAAGTGAAC ACCCTGACAGGAATGATT GTGTTGCCGTGCTCAG/A	Frameshift	ANKRD37	L19-1	AKFLTTIKCMQTTETESRKCRKYQW	S19-1	KYQWEKEVL	0,17
				L19-2	TIKCMQTTETESRKCRKYQWEKEVL	S19-2	RYYCLNVPLW	
NIC6	chr5_141628580_G/A	Missense	HDAC3	L20	ESGRYYCLNVPLWDGIDDQSYKHLF	S20-1	YYCLNVPLWD	0,66
						S20-2	GRYYCLNVPLW	
						S20-3	RYYCLNVPLWD	
						S20-4	SGRYYCLNVPLW	

Table S2 | Mutant peptide sequences that were investigated for T cell reactivity. *(continued)*

Patient ID	Mutational position	Mutation type	Gene	SLP ID	Long sequences	SSP ID	Short sequences	ALT_ DNA
						S20-5	YYCLNVPLW	
						S20-6	QAYGYSGVSL	
NIC6	chr6_169222303_C/T	Missense	THBS2	L21	QVTQTYWEDQPTQAYGYSGVSLKVV			0,66
NIC6	chr6_31161939_C/T	Missense	TCF19	L22	AELDDESEPPENLPPVLMEPRKKLR			0,39
NIC6	chrM_15062_T/C	Missense	MT-CYB	L23	LFLHIGRGLYYGPFLYSETWNIGII	S23-1	YYGPFLYSETW	0,88
						S23-2	LYYGPFLYSETW	
						S23-3	YYGPFLYSETWN	
						S23-4	FLYSETWNI	
						S23-5	YSETWNIGI	
NIC7	chr1_166858202_C/A	Missense	TADA1	L01	SHPPPDDAEQQASLLLACSGDTLPA	S01	AEQQASLLL	0,32
NIC7	chr1_173984497_A/T	Splice	RC3H1	L02-1	LALYLKPLSSARGKFVFVSYLKSKT			0,16
				L02-2	RGKFVFVSYLKSKTAFFKYSVHNPI			
NIC7	chr1_206195806_A/C	Missense	FAM72A	L03	CSSCLLSCNNGHVWMFHSQAVYDIN	S03-1	GHVWMFHSQAVY	0,30
						S03-2	CNNGHVWMF	
						S03-3	SCNNGHVWMF	
						S03-4	VWMFHSQAV	
						S03-5	VWMFHSQAVY	
						S03-6	HVWMFHSQAVY	
NIC7	chr1_224294313_C/T	Missense	NVL	L04	SLDPALRRAGRFNREICLGIPDEAS	S04-1	NREICLGIPD	0,33
						S04-2	NREICLGIPDEA	
						S04-3	NREICLGIPDE	
						S04-4	FNREICLGIPDE	
						S04-5	FNREICLGI	
						S04-6	RAGRFNREI	
NIC7	chr1_32091892_C/T	Missense	TMEM39B	L05-1	AMPTHACCLSPSFIRSEVEFLKMDF	S05-1	SPSFIRSEV	0,26
				L05-2	AHKTAVWPGRHAHPCLLPVTQLHPQ	S05-2	MPTHACCLSPSF	
						S05-3	SFIRSEVEF	

Table S2 | Mutant peptide sequences that were investigated for T cell reactivity. *(continued)*

Patient ID	Mutational position	Mutation type	Gene	SLP ID	Long sequences	SSP ID	Short sequences	ALT_ DNA
						S05-4	HACCLSPSFI	
						S05-5	LPVTQLHP	
						S05-6	LPVTQLHPQ	
NIC7	chr1_51302546_G/A	Missense	TTC39A	L06	FVLGTGNVNIEEVEKLLKPYLNRYP	S06	VEKLLKPYL	0,32
NIC7	chr1_7778152_T/TCAG	Inframe insertion	VAMP3	L07	KMWAIGITVLVIFSIIIIIVWVVSS	S07	VIFSIIIII	0,29
NIC7	chr10_112425377_T/G	Missense	ACSL5	L08	GTLKIIDRKKNIVKLAQGEYIAPEK	S08-1	IVKLAQGEY	0,29
						S08-2	VKLAQGEYI	
NIC7	chr10_472477_C/A	Missense	DIP2C	L09	PVTPSSASRYHRLRSSGSRDERYRS	S09	SSASRYHRL	0,54
NIC7	chr10_47922844_G/T	Missense	CH17-360D5.1	L10	FAVLWLPLHVFNILEDWHHEAIPIC	S10-1	LPLHVFNI	0,17
						S10-2	ILEDWHHEAI	
						S10-3	WLPLHVFNIL	
						S10-4	HVFNILEDW	
						S10-5	LPLHVFNIL	
NIC7	chr10_50814032_G/A	Missense	A1CF	L11-1	RAIIRAPSVRGAVGVRGLGGRGYLA	S11-1	VPVGAVGV	0,27
				L11-2	VREIYMNVPVGAVGVRGLGGRGYLA			
NIC7	chr11_59152054_G/A	Missense	FAM111A	L12	EIETHQGQEMLVHGTEGIKEYINLG	S12-1	QEMLVHGTE	0,25
						S12-2	GQEMLVHGTE	
						S12-3	MLVHGTEGI	
						S12-4	QEMLVHGTEGI	
						S12-5	GQEMLVHGTEGI	
NIC7	chr12_16363960_T/G	Missense	MGST1	L13	HTIAYLTPLPQPKRALSFFVGYGVT	S13-1	TPLPQPKRA	0,29
						S13-2	LPQPKRALSF	
						S13-3	LPQPKRALSFFV	
NIC7	chr12_1754359_GAA/G	Frameshift	ADIPOR2	L14-1	MNEPTAPIGVQQDSRARYKAQKRAP	S14-1	GVQQDSRARY	0,20
				L14-2	IGVQQDSRARYKAQKRAPTGWYTKR	S14-2	RAPTGWYTK	

Table S2 | Mutant peptide sequences that were investigated for T cell reactivity. *(continued)*

Patient ID	Mutational position	Mutation type	Gene	SLP ID	Long sequences	SSP ID	Short sequences	ALT_ DNA
						S14-3	NEPTAPIGV	
						S14-4	AQKRAPTGW	
NIC7	chr12_56257327_G/A	Missense	ANKRD52	L15	LDQERRTPLHAAVYVGDVPILQLLL	S15-1	TPLHAAVYV	0,06
						S15-2	PLHAAVYV	
						S15-3	AVYVGDVPI	
NIC7	chr13_109783442_C/T	Missense	IRS2	L16	TQPPHPVVPSPVQPSGGRPEGFLGQ	S16	VPSPVQPSG	0,07
NIC7	chr13_113766192_G/A	Missense	TMEM255B	L17	GSLLLVSVLIVTIGLAATTRTENVT	S17-1	SVLIVTIGL	0,18
						S17-2	LVSVLIVTI	
NIC7	chr16_72950933_C/T	Missense	ZFHX3	L18-1	LVGGEIPLDMRLRGGQLVSEELMNL	S18-1	GEIPLDMRLR	0,54
				L18-2	MRLRGGQLVSEELMNLGESFIQTND			
NIC7	chr17_7676002_TCA/T	Frameshift	TP53	L19-1	RLGFLHSGTAKSDLHVLPCPQQDVL	S19-1	LPCPQQDVL	0,21
				L19-2	SDLHVLPCPQQDVLPTGQDLPCAAV	S19-2	LPCPQQDV	
				L19-3	DLHVLPCPQQDVLPTGQDLPCAAVG	S19-3	TAKSDLHVL	
				L19-4	YQGSYGFRLGFLHSGTAKSDLHVLP			
				L19-5	RLGFLHSGTAKSDLHDVLPTGQDLP			
				L19-6	HSGTAKSDLHDVLPTGQDLPCAAVG			
NIC7	chr19_39879805_G/A	Missense	FCGBP	L20	GGQGVCLPNYEAMCWLWGDPHYHSF	S20-1	LPNYEAMCWL	0,13
						S20-2	LPNYEAMCW	
NIC7	chr19_55093057_C/T	Missense	PPP1R12C	L21	KPAQSLDPSRRPHVPGVENSDSPAQ			0,62
NIC7	chr2_240464953_C/A	Missense	GPC1	L22	RRRGKLAPRERPHSGTLEKLVSEAK	S22	RERPHSGTL	0,22
NIC7	chr20_34776325_C/T	Missense	NCOA6	L23	LRILAQSNNQQLQDLGILSVQIEGE	S23-1	QQLQDLGIL	0,16
						S23-2	LQDLGILSV	
NIC7	chr20_35044541_A/C	Missense	TRPC4AP	L24	TLLAKNAQQKKSVSLGPSAAEINQA	S24	AQQKKSVSL	0,14
NIC7	chr22_17108607_C/T	Missense	IL17RA	L25	TRAKWQALLGRGVPVRLRCDHGKPV	S25	ALLGRGVPV	0,46
NIC7	chr3_101857345_G/T	Missense	NFKBIZ	L26	TALHVAASLQYRFTQLDAVRLLMRK	S26	VAASLQYRF	0,04
NIC7	chr4_13602515_C/T	Missense	BOD1L1	L27	KYAETVKLKHKRNPGKVKDISIDVE			0,30
NIC7	chr7_129413686_G/A	Missense	AHCYL2	L28	VCNMGHSNTEIDMASLRTPELTWER	S28	MASLRTPEL	0,20

Table S2 | Mutant peptide sequences that were investigated for T cell reactivity. *(continued)*

Patient ID	Mutational position	Mutation type	Gene	SLP ID	Long sequences	SSP ID	Short sequences	ALT_ DNA
NIC7	chr8_66429486_C/A	Missense	RRS1	L29	RPRPLTRWQQFAILKGIRPKKKTNL			0,17
NIC7	chrM_15617_G/A	Missense	MT-CYB	L30	TILRSVPNKLGGILALLLSILILAM	S30-1	KLGGILALL	0,33
						S30-2	GILALLLSI	
NIC7	chrM_15617_G/A	Missense	MT-CYB	L30	TILRSVPNKLGGILALLLSILILAM	S30-3	LALLLSILI	
NIC7	chrX_54541327_C/T	Missense	GNL3L	L31	KQQAAREQERQKCRTIESYCQDVLR	S31	CRTIESYCQDVL	0,85
NIC7	chr19_48195980_G/A	Missense	C19orf68	L32	WRGAQLHDERAGELRTAEWKGPQSE	S32	GELRTAEWK	0,07
NIC7	chr1_18910469_C/T	Missense	IFFO2	L33-1	CNPTIDLQGELKLATAKSDMNRHLH	S33-1	GELKLATAK	0,30
				L33-2	KEYQETIGQIELKLATAKSDMNRHL	S33-2	QETIGQIELK	
						S33-3	TIDLQGELK	
						S33-4	IDLQGELKL	
NIC15	chr11_128489485_G/A	Missense	ETS1	L01	KEQQRLGIPKDPWQWTETHVRDWVM	S01.1	DPWQWTETHV	0,15
						S01.2	IPKDPWQW	
						S01.3	GIPKDPWQW	
NIC15	chr11_47168189_G/T	Missense	ARFGAP2	L02	EMQVIEQETPVSEKSSRSQLDLFDD	S02.1	SEKSSRSQL	0,17
						S02.2	SEKSSRSQLD	
						S02.3	SEKSSRSQLDLF	
						S02.4	QVIEQETPVSEK	
NIC15	chr12_49002999_C/T	Missense	PRKAG1	L03	TIINRLVEAEVHQLVVVDENDVVKG	S03.1	LVEAEVHQL	0,26
						S03.2	AEVHQLVVV	
						S03.3	EAEVHQLVV	
						S03.4	VEAEVHQLV	
						S03.5	VEAEVHQLVV	
						S03.6	AEVHQLVV	
						S03.7	EAEVHQLV	
						S03.8	EVHQLVVV	
						S03.9	VEAEVHQL	
NIC15	chr16_68234043_T/G	Missense	ESRP2	L04	ALLGGGPYMLCTAGQQLLRQVLHPE	S04.1	PYMLCTAGQQL	0,39

Table S2 | Mutant peptide sequences that were investigated for T cell reactivity. *(continued)*

Patient ID	Mutational position	Mutation type	Gene	SLP ID	Long sequences	SSP ID	Short sequences	ALT_ DNA
						S04.2	PYMLCTAGQQLL	
						S04.3	CTAGQQLLR	
NIC15	chr17_7673776_G/A	Missense	TP	L05	FEVRVCACPGRDWRTEEENLRKKGE	S05.1	VCACPGRDW	0,73
						S05.2	RVCACPGRDW	
NIC15	chr19_14409633_C/T	Missense	DDX39A	L06	LDVLEFNQVIIFIKSVQRCMALAQL	S06.1	IIFIKSVQR	0,18
						S06.10	FIKSVQRCM	
						S06.11	EFNQVIIFI	
						S06.12	QVIIFIKSV	
						S06.2	IKSVQRCMAL	
						S06.3	LEFNQVIIFI	
						S06.4	VIIFIKSVQR	
						S06.5	FIKSVQRCMAL	
						S06.6	IKSVQRCMALA	
						S06.7	FIKSVQRCMALA	
						S06.8	IFIKSVQRCMAL	
						S06.9	IKSVQRCMALAQ	
NIC15	chr19_56547529_G/A	Missense	ZFP28	L07	KAMSQGLVTFGDMAVDFSQEEWEWL	S07.1	TFGDMAVDF	0,21
						S07.2	MAVDFSQEEW	
						S07.3	VTFGDMAVDF	
						S07.4	GDMAVDFSQEEW	
						S07.5	FGDMAVDF	
						S07.6	FGDMAVDFS	
						S07.7	MAVDFSQEE	
						S07.8	VTFGDMAV	
						S07.9	LVTFGDMAV	
NIC15	chr20_63695080_G/T	Missense	RTEL1-TNFRSF6B	L08	EDFPLLHRFSMFLRPHHKQRFSQTC	S08.1	SMFLRPHHK	0,12

Table S2 | Mutant peptide sequences that were investigated for T cell reactivity. *(continued)*

Patient ID	Mutational position	Mutation type	Gene	SLP ID	Long sequences	SSP ID	Short sequences	ALT_ DNA
						S08.10	SMFLRPHHKQRF	
						S08.11	LLHRFSMFL	
						S08.2	FSMFLRPHHK	
						S08.3	LLHRFSMFLR	
						S08.4	FPLLHRFSMFL	
						S08.5	MFLRPHHKQRF	
						S08.6	RFSMFLRPHHK	
						S08.7	DFPLLHRFSMFL	
						S08.8	FPLLHRFSMFLR	
						S08.9	HRFSMFLRPHHK	
NIC15	chr2_152148109_C/A	Missense	STAM2	L09	HVALQALTLLGAFVANCGKIFHLEV	S09.1	GAFVANCGK	0,39
						S09.2	TLLGAFVANCGK	
						S09.3	FVANCGKIF	
						S09.4	AFVANCGKIF	
NIC15	chr2_165764976_G/A	Missense	GALNT3	L10	TSVIIVFHNEAWFTLLRTVHSVLYS	S10.1	VFHNEAWFTL	0,10
						S10.10	VFHNEAWF	
						S10.11	AWFTLLRTV	
						S10.2	EAWFTLLRTV	
						S10.3	IVFHNEAWFTL	
						S10.4	VFHNEAWFTLL	
						S10.5	IIVFHNEAWFTL	
						S10.6	VFHNEAWFTLLR	
						S10.7	FHNEAWFTL	
						S10.8	IVFHNEAWF	
						S10.9	NEAWFTLLR	
NIC15	chr3_49057146_C/A	Missense	QRICH1	L11	VHVSGSPTALAAFKLEDDKEKMVGT	S11.1	GSPTALAAFK	0,14
						S11.2	ALAAFKLEDDK	

Table S2 | Mutant peptide sequences that were investigated for T cell reactivity. *(continued)*

Patient ID	Mutational position	Mutation type	Gene	SLP ID	Long sequences	SSP ID	Short sequences	ALT_ DNA
						S11.3	SGSPTALAAFK	
						S11.4	TALAAFKLEDDK	
NIC15	chr3_49057146_C/A	Missense	QRICH1	L11	VHVSGSPTALAAFKLEDDKEKMVGT	S11.5	VSGSPTALAAFK	
						S11.6	AAFKLEDDK	
						S11.7	PTALAAFKL	
						S11.8	TALAAFKL	
						S11.9	GSPTALAAF	
NIC15	chr5_112839514_TAAAAG/T	Missense	APC	L12	IGCNQTTQEADSANTLQIAEIKDWN	S12.1	LQIAEIKDW	0,45
						S12.2	TLQIAEIKDW	
NIC15	chr9_136504880_A/C	Missense	NOTCH1	L13	FLRELSRVLHTNGVFKRDAHGQQMI	S13.1	RVLHTNGVFK	0,33
						S13.2	SRVLHTNGVFK	
						S13.3	LSRVLHTNGVFK	
						S13.4	RVLHTNGVF	
						S13.5	VLHTNGVFK	
						S13.6	RVLHTNGVFKR	
NIC15	chrM_11271_T/C	Missense	MT-ND4	L14	PLLIALIYTHNTPGSLNILLLTLTA	S14.1	YTHNTPGSL	0,15
						S14.2	IYTHNTPGSL	
						S14.3	IYTHNTPGSLNI	
						S14.4	HNTPGSLNI	
						S14.5	TPGSLNIL	
						S14.6	TPGSLNILL	
NIC15	chrM_13540_T/C	Missense	MT-ND	L15	YSKDHIIETANMPYTNAWALSITLI	S15.1	MPYTNAWALSI	0,18
						S15.10	MPYTNAWALSIT	
						S15.11	NMPYTNAWALSI	
						S15.12	PYTNAWALSITL	
						S15.13	MPYTNAWA	
						S15.14	ANMPYTNAW	

Table S2 | Mutant peptide sequences that were investigated for T cell reactivity. *(continued)*

Patient ID	Mutational position	Mutation type	Gene	SLP ID	Long sequences	SSP ID	Short sequences	ALT_ DNA
						S15.15	MPYTNAWAL	
						S15.16	IETANMPY	
						S15.17	PYTNAWAL	
						S15.2	ANMPYTNAWA	
						S15.3	HIIETANMPY	
						S15.4	MPYTNAWALS	
						S15.5	NMPYTNAWAL	
						S15.6	PYTNAWALSI	
						S15.7	TANMPYTNAW	
						S15.8	PYTNAWALSIT	
						S15.9	IETANMPYTNAW	
NIC17	chr10_133370734_C/T	Missense	ECHS1	L01	PFASGANFEYIITEKRGKNNTVGLI			0,20
NIC17	chr10_72935651_C/A	Missense	PLA2G12B	L02	TLGCRPFMNSQRAAFICAEEEKEEL	S02	FMNSQRAAF	0,46
NIC17	chr1_116589057_C/T	Missense	IGSF3	L03	QVSKSKRTLTLVKNKPIQLNCSVKS	S03.01	LVKNKPIQL	0,22
						S03.02	VKNKPIQL	
NIC17	chr11_17169117_G/C	Missense	PIK3C2A	L04	SYPLTPATPFHPEGSLPIYRPVVST	S04.01	TPFHPEGSL	0,63
						S04.02	YPLTPATPFHPE	
						S04.03	HPEGSLPIY	
NIC17	chr11_2570678_G/C	Missense	KCNQ1	L05	VVFFGTEYVVRLCSAGCRSKYVGLW			0,30
NIC17	chr11_6683217_T/C	Missense	MRPL17	L06	FRRMGLGPESRIRLLRNLLTGLVRH	S06	SRIRLLRNL	0,43
NIC17	chr1_26122123_T/C	Missense	PDIK1L	L07.1	TSDLEPTLKVADSGLSKVCSASGQN			0,41
NIC17	chr1_26122123_T/C	Missense	PDIK1L	L07.2	PDNILISQTRLDTSDLEPTLKVADS			0,41
NIC17	chr12_6750194_G/A	Missense	MLF2	L08.1	GAPKVYQETSEMCSAPGGIRETRRT			0,13
NIC17	chr12_6750194_G/A	Missense	MLF2	L08.2	GAPKVYQETSEMCSAPGGVSWGALL			0,13
NIC17	chr13_102821834_A/G	Missense	BIVM	L09	FEDIRFGPFTGNATLMRWFRQINDH	S09.0	GPFTGNATL	0,75
						S09.01	FGPFTGNATL	
						S09.02	FGPFTGNATLM	

Table S2 | Mutant peptide sequences that were investigated for T cell reactivity. *(continued)*

Patient ID	Mutational position	Mutation type	Gene	SLP ID	Long sequences	SSP ID	Short sequences	ALT_ DNA
						S09.03	FGPFTGNATLMR	
						S09.04	IRFGPFTGNATL	
						S09.05	RFGPFTGNATLM	
						S09.06	PFTGNATL	
NIC17	chr13_30657546_C/T	Missense	USPL1	L10	CSERHKKFEVPALEIHIVIWERKIS	S10.01	KFEVPALEI	0,13
						S10.02	VPALEIHIVI	
NIC17	chr14_21230984_T/A	Missense	HNRNPC	L11.1	KRSAAEMYGSVTDHPSPSPLLSSSF			0,18
NIC17	chr14_21230984_T/A	Missense	HNRNPC	L11.2	KRSAAEMYGSVTDHPSPSPLLSVYQ			0,18
NIC17	chr1_44802975_G/A	Missense	PLK3	L12	SLGCVMYTLLCGNPPFETADLKETY	S12.01	NPPFETADL	0,27
						S12.02	TLLCGNPPF	
NIC17	chr15_44651635_G/C	Missense	SPG11	L13	ELKCVSVTGFTAVFTWEVERMGYTI	S13.01	VFTWEVERMGY	0,53
						S13.02	AVFTWEVERMGY	
						S13.03	VFTWEVERMGYT	
						S13.04	FTAVFTWEV	
NIC17	chr15_68086601_C/T	Missense	PIAS1	L14	PQLTYDGHPASSLLLPVSLLGPKHE	S14.01	TYDGHPASSL	0,50
						S14.02	HPASSLLLPVSL	
						S14.03	HPASSLLL	
NIC17	chr16_19699568_C/T	Missense	C16orf62	L15	SFFNSILAHGDLCNNKLNQLSVNLW			0,51
NIC17	chr16_2175867_G/T	Missense	TRAF7	L16	KIWDIRTLDCIHFLQTSGGSVYSIA	S16	RTLDCIHFL	0,31
NIC17	chr1_6469615_G/A	Missense	PLEKHG5	L17	TDLLLVTKAVKKVERTRVIRPPLLV			0,24
NIC17	chr16_67167533_C/T	Missense	HSF4	L18	GLSPHRARGPIIFDIPEDSPSPEGT	S18.01	HRARGPIIF	0,12
						S18.02	ARGPIIFDI	
NIC17	chr1_68137792_C/A	Missense	WLS	L19.1	FLYAPSHKNYGEYQSNGDLGVHSGE	S19	EYQSNGMQL	0,40
NIC17	chr1_68137792_C/A	Missense	WLS	L19.2	FLYAPSHKNYGEYQSNGMQLPCKSR			0,40
NIC17	chr17_82054677_G/A	Missense	GPS1	L20	NYKGNSIKESIRHGHDDLGDHYLDC	S20	HGHDDLGDHY	0,42
NIC17	chr18_58919969_C/T	Missense	ZNF532	L21	QQIKQAIINAAALQPPKKVSRVQVV	S21	QAIINAAAL	0,50
NIC17	chr19_11021837_C/T	Missense	SMARCA4	L22	NTHYVAPRRLLLMGTPLQNKLPELW	S22	VAPRRLLLM	0,35

Table S2 | Mutant peptide sequences that were investigated for T cell reactivity. *(continued)*

Patient ID	Mutational position	Mutation type	Gene	SLP ID	Long sequences	SSP ID	Short sequences	ALT_ DNA
NIC17	chr19_3478879_C/T	Missense	SMIM24	L23	LKPWLVGLAAVVSFLFIVYLVLLAN	S23	VSFLFIVYL	0,29
NIC17	chr19_47680387_G/T	Missense	GLTSCR1	L24	PQNLTFMAAGKAVQNVVLSGFPAPA			0,17
NIC17	chr19_55092787_G/A	Missense	PPP1R12C	L25	EHRKVGKEWRGPVEGEEAEPADRSQ			0,45
NIC17	chr19_55482650_A/C	Missense	ZNF628	L26	RDHTGERPYQCGACGKAFKRSSLLA			0,20
NIC17	chr20_63882783_G/C	Missense	TPD52L2	L27	QAGQKTSAALSTLGSAISRKLGDMR			0,16
NIC17	chr3_136152028_C/A	Missense	MSL2	L28	VLRSLETVSNTEFCCPNLQPNLEAT			0,17
NIC17	chr3_45500451_C/A	Missense	LARS2	L29	RYTDPHNPHSPFKTAVADYWMPVDL	S29.01	YTDPHNPHSPFK	0,15
						S29.02	SPFKTAVAD	
NIC17	chr4_143538936_A/C	Missense	SMARCA5	L30	DSDWNPQVDLQALDRAHRIGQTKTV	S30.01	NPQVDLQAL	0,25
						S30.02	QALDRAHRI	
NIC17	chr4_76740029_C/A	Missense	SHROOM3	L31	QAQAWQAGEDKRYSRLSEPWEGDFQ	S31.01	RYSRLSEPW	0,26
						S31.02	KRYSRLSEPW	
						S31.03	RYSRLSEPWE	
						S31.04	GEDKRYSRL	
NIC17	chr6_31888379_C/T	Missense	EHMT2	L32	ARMVKHHCCPGCDYFCTAGTFLECH	S32.01	CDYFCTAGTF	0,03
						S32.02	DYFCTAGTF	
NIC17	chr7_117791275_C/A	Missense	CTTNBP2	L33	SALATSQVGAWPSATPGLNQPACSD	S33	AWPSATPGL	0,40
NIC17	chr7_135209655_C/T	Missense	WDR91	L34	DYWSYLERRLFSHLEDIYRPTIHKL	S34.01	YLERRLFSHL	0,14
						S34.02	WSYLERRLFSHL	
						S34.03	RLFSHLEDI	
NIC17	chr7_143291622_T/A	Missense	CASP2	L35	KKNRVVLAKQLLMSELLEHLLEKDI	S35	VVLAKQLLM	0,09
NIC17	chr7_4788195_C/A	Missense	AP5Z1	L36	APAASERPLWDTYLRAPSCLEAFRD	S36.01	ASERPLWDTY	0,12
						S36.02	AASERPLWDTY	
						S36.03	PAASERPLWDTY	
						S36.04	TYLRAPSCLEAF	
						S36.05	ERPLWDTYL	
						S36.06	TYLRAPSCL	

Table S2 | Mutant peptide sequences that were investigated for T cell reactivity. *(continued)*

Patient ID	Mutational position	Mutation type	Gene	SLP ID	Long sequences	SSP ID	Short sequences	ALT_ DNA
NIC17	chr7_5715168_C/T	Missense	RNF216	L37	EQYQKDGQLIECHCCYGEFPFEELT			0,35
NIC17	chr7_756863_A/T	Missense	DNAAF5	L38	VFLKLILSTLKKSPSASGLLVLASA	S38.01	SPSASGLLVL	0,13
						S38.02	SPSASGLLV	
NIC17	chr7_99035681_G/C	Missense	SMURF1	L39	ELIIGGLDKIDLKDWKSNTRLKHCV			0,12
NIC17	chr9_131475787_G/A	Missense	PRRC2B	L40	RLSNCGYGRRTFISKESPHWQSKSP	S40	CGYGRRTFI	0,62
NIC17	chr9_72916962_G/C	Missense	ALDH1A1	L41	FVRRSVERAKKYMLGNPLTPGVTQG	S41	ERAKKYML	0,21
NIC17	chr9_87706564_G/A	Missense	DAPK1	L42	CRWIHQQSTEGDTDIRLWVNGCKLA			0,55
NIC17	chrX_64921864_TC/T	Frameshift	ZC4H2	L43	YKQEMDLLLQEKWPMWRNSD	S43.01	LLQEKWPM	0,77
						S43.02	LLLQEKWPM	

Table S3 | Immune-regulatory gene set.

Gene	Entrez	Gene	Entrez
ADORA2A	135	*ICOS*	29851
ARG1	383	*ICOSLG*	23308
BTLA	151888	*IDO1*	3620
C10orf54	64115	*IFI6*	3428
CCL5	6352	*IFNA1*	3439
CD27	939	*IFNA2*	3440
CD274	29126	*IFNG*	3458
CD276	80381	*IL10*	3586
CD28	940	*IL12A*	3592
CD40	958	*IL13*	3596
CD40LG	959	*IL1A*	3552
CD70	970	*IL1B*	3553
CD80	941	*IL2*	3558
CIITA	4261	*IL2RA*	3559
CTLA4	1493	*IL4*	3565
CX3CL1	6376	*ITGB2*	3689
CXCL10	3627	*KIR2DL1*	3802
CXCL9	4283	*KIR2DL2*	3803
ENTPD1	953	*KIR2DL3*	3804
FOXP3	50943	*LAG3*	3902
GZMA	3001	*MICA*	100507436
GZMA	3001	*MICB*	4277
HAVCR2	84868	*PDCD1*	5133
HLA-A	3105	*PDCD1LG2*	80380
HLA-B	3106	*PRF1*	5551
HLA-C	3107	*SELP*	6403
HLA-DPA1	3113	*TGFB1*	7040
HLA-DPB1	3115	*TIGIT*	201633
HLA-DQA1	3117	*TLR4*	7099
HLA-DQA2	3118	*TNF*	7124
HLA-DQB1	3119	*TNFRSF14*	8764
HLA-DQB2	3120	*TNFRSF18*	8784
HLA-DRA	3122	*TNFRSF4*	7293
HLA-DRB1	3123	*TNFRSF9*	3604
HLA-DRB3	3125	*TNFSF4*	7292
HLA-DRB4	3126	*TNFSF9*	8744
HLA-DRB5	3127	*VEGFA*	7422
HMGB1	3146	*VEGFB*	7423
ICAM1	3383	*VTCN1*	79679

Table S4 | Antibody panels used for flow cytometric analyses.

A. T cell phenotyping panel										
Antibody	Fluorochrome	Dilution	Company	Order number	Isotype	Clone	Laser	Wavelength	Mirror	Filter
CD4	Pacific Blue	1:800	BD	558116	Mouse IgG1, κ	RPA-T4	Violet	405nm	-	450/50
CD8	Pacific Orange	1:200	ThermoFisher	MHCD0830	Mouse IgG2a	3B5	Violet	405nm	505LP	525/50
CD45RA	FITC	1:30	BD	335039	Mouse IgG1, κ	L48	Blue	488nm	505LP	530/30
CD45RO	PerCP-Cy5.5	1:20	Sony Biotechnology	2121110	Mouse IgG2a,κ	UCHL1	Blue	488nm	685LP	710/50
CD103	BV650	1:75	BioLegend	350218	Mouse IgG1, κ	Ber-ACT8	Violet	405nm	630LP	670/30
CD39	APC	1:60	BioLegend	328210	Mouse IgG1	A1	Red	640nm	665LP	670/14
PD-1	PE	1:30	eBioscience	12-9969-42	Mouse IgG1, κ	MIH4	Yellow Green	561nm	-	582/15
FoxP3	PE-CF594	1:150	BD	562421	Mouse IgG1	259D/C7	Yellow Green	561nm	600LP	610/20
Live/dead	nIR	1:10	ThermoFisher	L10119	-	-	Red	640nm	750LP	780/60
B. T cell reactivity panel										
Antibody	Fluorochrome	Dilution	Company	Order number	Isotype	Clone	Laser	Wavelength	Mirror	Filter
CD3	Horizon-V450	1:40	BD	560365	Mouse IgG1, κ	UCHT1	Violet	405nm	-	450/50
CD4	PE-CF594	1:50	BD	562281	Mouse IgG1, κ	RPA-T4	Yellow Green	561nm	600LP	610/20
CD8	APC-Cy7	1:40	BD	348813	Mouse IgG1, κ	SK1	Red	640nm	750LP	780/60
CD137	APC	1:100	BD	550890	Mouse IgG1, κ	4B4-1	Red	640nm	665LP	670/14
Live/dead	Yellow-Ard	1:800	ThermoFisher	L34959	-	-	Violet	405nm	570LP	585/15

Table S5 | Phenotypic analysis of the expanded TIL products.

				% of CD4/CD8					
Patient ID	TIL yield (x106)	Expansion rate	CD4/CD8 (%)	CD45RO	PD-1	CD39-CD103-	CD39-CD103+	CD39+CD103-	CD39+CD103+
NIC3	11	1012	95/5	99/100	4/0.4	2/1	0/0.1	97/40	1/57
NIC4	35	951	81/19	99/100	12/6	40/16	0.3/1	56/56	1/24
NIC5	18	6.3	93/7	94/98	21/11	20/13	0.4/3	70/38	4/43
NIC6	2	515	97/3	97/99	11/1	20/9	0/1	76/59	0.2/30
NIC7	5	783	92/8	99/99	23/3	7/5	0/1	90/62	2/31
NIC13	33	691	84/16	100/100	12/0.8	15/3	0/0	83/82	0/13
NIC15	55	744	69/31	99/100	28/2	8/61	0/0	90/32	0.1/0.3
NIC17	35	413	34/66	97/98	12/4	51/17	0/0.1	44/77	0/1

REFERENCES

1. Bray F, Ferlay J, Soerjomataram I, Siegel RL, Torre LA, Jemal A. Global cancer statistics 2018: GLOBOCAN estimates of incidence and mortality worldwide for 36 cancers in 185 countries. CA: A Cancer Journal for Clinicians. 2018;68(6):394-424.
2. Le DT, Uram JN, Wang H, Bartlett BR, Kemberling H, Eyring AD, et al. PD-1 Blockade in Tumors with Mismatch-Repair Deficiency. New England Journal of Medicine. 2015;372(26):2509-20.
3. Yarchoan M, Johnson BA, 3rd, Lutz ER, Laheru DA, Jaffee EM. Targeting neoantigens to augment antitumour immunity. Nature reviews Cancer. 2017;17(4):209-22.
4. Le DT, Durham JN, Smith KN, Wang H, Bartlett BR, Aulakh LK, et al. Mismatch-repair deficiency predicts response of solid tumors to PD-1 blockade. Science (New York, NY). 2017;357(6349):409-13.
5. Domingo E, Freeman-Mills L, Rayner E, Glaire M, Briggs S, Vermeulen L, et al. Somatic POLE proofreading domain mutation, immune response, and prognosis in colorectal cancer: a retrospective, pooled biomarker study. The Lancet Gastroenterology & Hepatology. 2016;1(3):207-16.
6. Snyder A, Makarov V, Merghoub T, Yuan J, Zaretsky JM, Desrichard A, et al. Genetic basis for clinical response to CTLA-4 blockade in melanoma. The New England journal of medicine. 2014;371(23):2189-99.
7. van Rooij N, van Buuren MM, Philips D, Velds A, Toebes M, Heemskerk B, et al. Tumor exome analysis reveals neoantigen-specific T-cell reactivity in an ipilimumab-responsive melanoma. Journal of clinical oncology : official journal of the American Society of Clinical Oncology. 2013;31(32):e439-42.
8. Van Allen EM, Miao D, Schilling B, Shukla SA, Blank C, Zimmer L, et al. Genomic correlates of response to CTLA-4 blockade in metastatic melanoma. Science (New York, NY). 2015;350(6257):207-11.
9. Samstein RM, Lee C-H, Shoushtari AN, Hellmann MD, Shen R, Janjigian YY, et al. Tumor mutational load predicts survival after immunotherapy across multiple cancer types. Nature Genetics. 2019;51(2):202-6.
10. McGranahan N, Furness AJ, Rosenthal R, Ramskov S, Lyngaa R, Saini SK, et al. Clonal neoantigens elicit T cell immunoreactivity and sensitivity to immune checkpoint blockade. Science (New York, NY). 2016;351(6280):1463-9.
11. Rizvi NA, Hellmann MD, Snyder A, Kvistborg P, Makarov V, Havel JJ, et al. Cancer immunology. Mutational landscape determines sensitivity to PD-1 blockade in non-small cell lung cancer. Science (New York, NY). 2015;348(6230):124-8.
12. Guinney J, Dienstmann R, Wang X, de Reynies A, Schlicker A, Soneson C, et al. The consensus molecular subtypes of colorectal cancer. Nat Med. 2015;21(11):1350-6.
13. Calon A, Lonardo E, Berenguer-Llergo A, Espinet E, Hernando-Momblona X, Iglesias M, et al. Stromal gene expression defines poor-prognosis subtypes in colorectal cancer. Nat Genet. 2015;47(4):320-9.
14. Trombetta ES, Mellman I. CELL BIOLOGY OF ANTIGEN PROCESSING IN VITRO AND IN VIVO. Annual Review of Immunology. 2004;23(1):975-1028.
15. Yewdell JW, Reits E, Neefjes J. Making sense of mass destruction: quantitating MHC class I antigen presentation. Nature reviews Immunology. 2003;3(12):952-61.

16. Ott PA, Hu Z, Keskin DB, Shukla SA, Sun J, Bozym DJ, et al. An immunogenic personal neoantigen vaccine for patients with melanoma. Nature. 2017;547(7662):217-21.

17. Scheper W, Kelderman S, Fanchi LF, Linnemann C, Bendle G, de Rooij MAJ, et al. Low and variable tumor reactivity of the intratumoral TCR repertoire in human cancers. Nat Med. 2019;25(1):89-94.

18. Verdegaal EM, de Miranda NF, Visser M, Harryvan T, van Buuren MM, Andersen RS, et al. Neoantigen landscape dynamics during human melanoma-T cell interactions. Nature. 2016;536(7614):91-5.

19. Li H, Durbin R. Fast and accurate short read alignment with Burrows–Wheeler transform. Bioinformatics. 2009;25(14):1754-60.

20. Picard Toolkit. http://broadinstitute.github.io/picard/: Broad Institute, GitHub Repository; 2019.

21. Szolek A, Schubert B, Mohr C, Sturm M, Feldhahn M, Kohlbacher O. OptiType: precision HLA typing from next-generation sequencing data. Bioinformatics (Oxford, England). 2014;30(23):3310-6.

22. Cibulskis K, Lawrence MS, Carter SL, Sivachenko A, Jaffe D, Sougnez C, et al. Sensitive detection of somatic point mutations in impure and heterogeneous cancer samples. Nature biotechnology. 2013;31(3):213-9.

23. Koboldt DC, Zhang Q, Larson DE, Shen D, McLellan MD, Lin L, et al. VarScan 2: somatic mutation and copy number alteration discovery in cancer by exome sequencing. Genome research. 2012;22(3):568-76.

24. Saunders CT, Wong WSW, Swamy S, Becq J, Murray LJ, Cheetham RK. Strelka: accurate somatic small-variant calling from sequenced tumor–normal sample pairs. Bioinformatics. 2012;28(14):1811-7.

25. McKenna A, Hanna M, Banks E, Sivachenko A, Cibulskis K, Kernytsky A, et al. The Genome Analysis Toolkit: a MapReduce framework for analyzing next-generation DNA sequencing data. Genome research. 2010;20(9):1297-303.

26. Robinson JT, Thorvaldsdóttir H, Winckler W, Guttman M, Lander ES, Getz G, et al. Integrative genomics viewer. Nature biotechnology. 2011;29:24.

27. Thorvaldsdóttir H, Robinson JT, Mesirov JP. Integrative Genomics Viewer (IGV): high-performance genomics data visualization and exploration. Briefings in Bioinformatics. 2013;14(2):178-92.

28. Robinson JT, Thorvaldsdóttir H, Wenger AM, Zehir A, Mesirov JP. Variant Review with the Integrative Genomics Viewer. Cancer Research. 2017;77(21):e31-e4.

29. McLaren W, Gil L, Hunt SE, Riat HS, Ritchie GRS, Thormann A, et al. The Ensembl Variant Effect Predictor. Genome Biology. 2016;17(1):122.

30. Wu TD, Watanabe CK. GMAP: a genomic mapping and alignment program for mRNA and EST sequences. Bioinformatics. 2005;21(9):1859-75.

31. Favero F, Joshi T, Marquard AM, Birkbak NJ, Krzystanek M, Li Q, et al. Sequenza: allele-specific copy number and mutation profiles from tumor sequencing data. Annals of Oncology. 2014;26(1):64-70.

32. Andreatta M, Nielsen M. Gapped sequence alignment using artificial neural networks: application to the MHC class I system. Bioinformatics (Oxford, England). 2016;32(4):511-7.

33. Nielsen M, Lundegaard C, Worning P, Lauemoller SL, Lamberth K, Buus S, et al. Reliable prediction of T-cell epitopes using neural networks with novel sequence representations. Protein science : a publication of the Protein Society. 2003;12(5):1007-17.

34. Jurtz V, Paul S, Andreatta M, Marcatili P, Peters B, Nielsen M. NetMHCpan-4.0: Improved Peptide-MHC Class I Interaction Predictions Integrating Eluted Ligand and Peptide Binding Affinity Data. Journal of immunology (Baltimore, Md : 1950). 2017;199(9):3360-8.

35. Eide PW, Bruun J, Lothe RA, Sveen A. CMScaller: an R package for consensus molecular subtyping of colorectal cancer pre-clinical models. Sci Rep. 2017;7(1):16618.

36. Anders S, Pyl PT, Huber W. HTSeq—a Python framework to work with high-throughput sequencing data. Bioinformatics (Oxford, England). 2014;31(2):166-9.

37. Robinson MD, McCarthy DJ, Smyth GK. edgeR: a Bioconductor package for differential expression analysis of digital gene expression data. Bioinformatics (Oxford, England). 2009;26(1):139-40.

38. Ritchie ME, Phipson B, Wu D, Hu Y, Law CW, Shi W, et al. limma powers differential expression analyses for RNA-sequencing and microarray studies. Nucleic Acids Research. 2015;43(7):e47-e.

39. Gros A, Parkhurst MR, Tran E, Pasetto A, Robbins PF, Ilyas S, et al. Prospective identification of neoantigen-specific lymphocytes in the peripheral blood of melanoma patients. Nat Med. 2016;22(4):433-8.

40. Duhen T, Duhen R, Montler R, Moses J, Moudgil T, de Miranda NF, et al. Co-expression of CD39 and CD103 identifies tumor-reactive CD8 T cells in human solid tumors. Nature communications. 2018;9(1):2724.

41. Ijsselsteijn ME, Petitprez F, Lacroix L, Ruano D, van der Breggen R, Julie C, et al. Revisiting immune escape in colorectal cancer in the era of immunotherapy. British journal of cancer. 2019.

42. Ijsselsteijn ME, Brouwer TP, Abdulrahman Z, Reidy E, Ramalheiro A, Heeren AM, et al. Cancer immunophenotyping by seven-colour multispectral imaging without tyramide signal amplification. The journal of pathology Clinical research. 2018;5(1):3-11.

43. Gros A, Tran E, Parkhurst MR, Ilyas S, Pasetto A, Groh EM, et al. Recognition of human gastrointestinal cancer neoantigens by circulating PD-1+ lymphocytes. The Journal of clinical investigation. 2019.

44. Thommen DS, Koelzer VH, Herzig P, Roller A, Trefny M, Dimeloe S, et al. A transcriptionally and functionally distinct PD-1(+) CD8(+) T cell pool with predictive potential in non-small-cell lung cancer treated with PD-1 blockade. Nat Med. 2018;24(7):994-1004.

45. Parkhurst MR, Robbins PF, Tran E, Prickett TD, Gartner JJ, Jia L, et al. Unique neoantigens arise from somatic mutations in patients with gastrointestinal cancers. Cancer discovery. 2019:CD-18-1494.

46. Verdegaal EME, Hoogstraten C, Sandel MH, Kuppen PJK, Brink AATP, Claas FHJ, et al. Functional CD8+ T cells infiltrate into nonsmall cell lung carcinoma. Cancer Immunology, Immunotherapy. 2007;56(5):587-600.

47. Simoni Y, Becht E, Fehlings M, Loh CY, Koo S-L, Teng KWW, et al. Bystander CD8+ T cells are abundant and phenotypically distinct in human tumour infiltrates. Nature. 2018;557(7706):575-9.

48. Kondo K, Okuma K, Tanaka R, Zhang LF, Kodama A, Takahashi Y, et al. Requirements for the functional expression of OX40 ligand on human activated CD4+ and CD8+ T cells. Human Immunology. 2007;68(7):563-71.

49. Garo LP, Ajay AK, Fujiwara M, Beynon V, Kuhn C, Gabriely G, et al. Smad7 Controls Immunoregulatory PDL2/1-PD1 Signaling in Intestinal Inflammation and Autoimmunity. Cell Reports. 2019;28(13):3353-66.e5.

50. Li L, Yang L, Wang L, Wang F, Zhang Z, Li J, et al. Impaired T cell function in malignant pleural effusion is caused by TGF-β derived predominantly from macrophages. International journal of cancer. 2016;139(10):2261-9.

51. Chen W, Jin W, Hardegen N, Lei K-j, Li L, Marinos N, et al. Conversion of Peripheral CD4+CD25- Naive T Cells to CD4+CD25+ Regulatory T Cells by TGF-β Induction of Transcription Factor Foxp3. The Journal of Experimental Medicine. 2003;198(12):1875.

52. Zhang N, Bevan Michael J. Transforming Growth Factor-β Signaling Controls the Formation and Maintenance of Gut-Resident Memory T Cells by Regulating Migration and Retention. Immunity. 2013;39(4):687-96.

53. Kehrl JH, Wakefield LM, Roberts AB, Jakowlew S, Alvarez-Mon M, Derynck R, et al. Production of transforming growth factor beta by human T lymphocytes and its potential role in the regulation of T cell growth. The Journal of Experimental Medicine. 1986;163(5):1037.

54. Ranges GE, Figari IS, Espevik T, Palladino MA. Inhibition of cytotoxic T cell development by transforming growth factor beta and reversal by recombinant tumor necrosis factor alpha. The Journal of Experimental Medicine. 1987;166(4):991.

55. Thomas DA, Massague J. TGF-beta directly targets cytotoxic T cell functions during tumor evasion of immune surveillance. Cancer cell. 2005;8(5):369-80.

56. Dimeloe S, Gubser P, Loeliger J, Frick C, Develioglu L, Fischer M, et al. Tumor-derived TGF-beta inhibits mitochondrial respiration to suppress IFN-gamma production by human CD4(+) T cells. Science signaling. 2019;12(599).

57. Tauriello DVF, Palomo-Ponce S, Stork D, Berenguer-Llergo A, Badia-Ramentol J, Iglesias M, et al. TGFbeta drives immune evasion in genetically reconstituted colon cancer metastasis. Nature. 2018;554(7693):538-43.

58. Mariathasan S, Turley SJ, Nickles D, Castiglioni A, Yuen K, Wang Y, et al. TGFβ attenuates tumour response to PD-L1 blockade by contributing to exclusion of T cells. Nature. 2018;554:544.

59. Colak S, Ten Dijke P. Targeting TGF-beta Signaling in Cancer. Trends in cancer. 2017;3(1):56-71.

60. Batlle E, Massague J. Transforming Growth Factor-beta Signaling in Immunity and Cancer. Immunity. 2019;50(4):924-40.

61. Tran E, Ahmadzadeh M, Lu Y-C, Gros A, Turcotte S, Robbins PF, et al. Immunogenicity of somatic mutations in human gastrointestinal cancers. Science (New York, NY). 2015;350:1387-90.

62. Tran E, Robbins PF, Lu YC, Prickett TD, Gartner JJ, Jia L, et al. T-Cell Transfer Therapy Targeting Mutant KRAS in Cancer. N Engl J Med. 2016;375(23):2255-62.

63. Fontana E, Eason K, Cervantes A, Salazar R, Sadanandam A. Context matters-consensus molecular subtypes of colorectal cancer as biomarkers for clinical trials. Annals of oncology : official journal of the European Society for Medical Oncology. 2019;30(4):520-7.

64. Bobisse S, Genolet R, Roberti A, Tanyi JL, Racle J, Stevenson BJ, et al. Sensitive and frequent identification of high avidity neo-epitope specific CD8 (+) T cells in immunotherapy-naive ovarian cancer. Nature communications. 2018;9(1):1092.

65. Tanyi JL, Bobisse S, Ophir E, Tuyaerts S, Roberti A, Genolet R, et al. Personalized cancer vaccine effectively mobilizes antitumor T cell immunity in ovarian cancer. Science translational medicine. 2018;10(436).

66. Keskin DB, Anandappa AJ, Sun J, Tirosh I, Mathewson ND, Li S, et al. Neoantigen vaccine generates intratumoral T cell responses in phase Ib glioblastoma trial. Nature. 2019;565(7738):234-9.

67. Hilf N, Kuttruff-Coqui S, Frenzel K, Bukur V, Stevanovic S, Gouttefangeas C, et al. Actively personalized vaccination trial for newly diagnosed glioblastoma. Nature. 2019;565(7738):240-5.

68. Tran E, Turcotte S, Gros A, Robbins PF, Lu YC, Dudley ME, et al. Cancer immunotherapy based on mutation-specific CD4+ T cells in a patient with epithelial cancer. Science (New York, NY). 2014;344(6184):641-5.

69. van den Bulk J, Verdegaal EM, de Miranda NF. Cancer immunotherapy: broadening the scope of targetable tumours. Open biology. 2018;8(6).